

1 Cold Exposure Protects Against Medial Arterial Calcification Development via
2 Autophagy

3
4 Fu-Xing-Zi Li¹, Jun-Jie Liu², Feng Xu¹, Su-Kang Shan¹, Feng Xu¹, Ming-Hui
5 Zheng¹, Limin-Li-Min Lei¹, Xiao Lin³, Bei Guo¹, Changchun-Chang-Chun Li¹, Feng
6 Wu⁴, Kexin-Ke-Xin Tang¹, Yechi-Ye-Chi Cao¹, Yunyun-Yun-Yun Wu¹, Jiayue-Jia-Yue
7 Duan¹, Yanlin-Yan-Lin Wu¹, Siyang-Si-Yang He¹, Xi Chen¹ and Lingqing-Ling-Qing
8 Yuan^{1*}

9 ¹Department of Metabolism and Endocrinology, National Clinical Research Center for
10 Metabolic Disease, Hunan Provincial Key Laboratory of Metabolic Bone Diseases, The
11 Second Xiangya Hospital, Central South University, Changsha, China.

12 ²Department of Periodontal Division, Hunan Xiangya Stomatological Hospital, Central
13 South University, Changsha, China.

14 ³Department of Radiology, The Second Xiangya Hospital, Central South University,
15 Changsha, China.

16 ⁴Department of Pathology, The Second Xiangya Hospital, Central South University,
17 Changsha, China.

18
19 **Abstract**

20 Medial arterial calcification (MAC), a systemic vascular disease different from
21 atherosclerosis, is associated with an increased incidence of cardiovascular events.
22 Several studies have demonstrated that ambient temperature is one of the most
23 important factors affecting cardiovascular events. However, there has been limited
24 research on the effect of different ambient temperatures on MAC. In the present study,
25 we showed that ~~compared with room temperature exposure (RT)~~, cold temperature
26 exposure (CT) in mice ~~slowed down the formation of~~ ~~decreased~~ vitamin D (VD)-
27 induced vascular calcification ~~compared with room temperature exposure (RT)~~. To
28 investigate the mechanism involved, we isolated plasma-derived exosomes from mice
29 subjected to CT or RT for 30 days (CT-Exo or RT-Exo, respectively). Compared with
30 RT-Exo, CT-Exo remarkably ~~alleviate~~ ~~inhibited~~ the ~~senescence~~/calcification/~~senescence~~
31 ~~formation~~ of vascular smooth muscle cells (VSMCs) and promoted autophagy by
32 activating ~~the~~ phosphorylation of AMP-activated protein kinase (p-AMPK) and
33 inhibiting phosphorylation of mammalian target of rapamycin (p-mTOR). At the same
34 time, CT-Exo promoted autophagy in β -glycerophosphate (β -GP)-induced VSMCs.
35 The number of autophagosomes and the expression of autophagy-related proteins ATG5
36 and LC3B increased, while the expression of p62 decreased. Based on a microRNA
37 chip microarray assay and real-time polymerase chain reaction, miR-320a-3p was
38 highly enriched in CT-Exo as well as thoracic aortic vessels in CT mice. miR-320a-3p
39 downregulation in CT-Exo using AntagomiR-320a-3p inhibited autophagy and blunted
40 its anti-calcification ~~protective~~ effect on VSMCs. Moreover, we identified that
41 programmed cell death 4 (PDCD4) is a target of miR-320a-3p, and silencing PDCD4
42 increased autophagy and decreased calcification in VSMCs. Treatment with CT-Exo
43 alleviated ~~the formation of~~ MAC in VD-treated mice, while these effects were partially

带格式的: 两端对齐

带格式的: 两端对齐

设置了格式: 上标

设置了格式: 上标

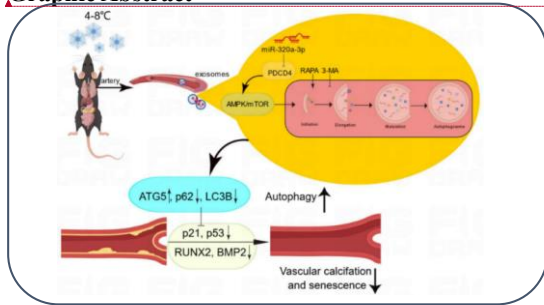
带格式的: 两端对齐

设置了格式: 非上标/ 下标

44 reversed by GW4869. Furthermore, the anti-arterial calcification protective effects of
45 CT-Exo were largely abolished by AntagomiR-320a-3p in VD-induced mice. In
46 summary, we have highlighted that prolonged cold may be a good way to reduce the
47 incidence of MAC. Specifically, miR-320a-3p from CT-Exo could protect against the
48 initiation and progression of MAC via the AMPK/mTOR autophagy pathway.

49
50 **Keywords:** Cold exposure, Arterial calcification, Plasma-derived exosomes,
51 Autophagy, Senescence, miR-320a-3p, PDCD4.

52 53 54 **Graphic Abstract**



设置了格式: 字体: 加粗

设置了格式: 字体: 加粗

带格式的: 缩进: 首行缩进: 0 字符

55 56 57 **Introduction**

58 The benefits of outdoor swimming in the winter and cold bathing are well known.
59 Indeed, the physiological response of humans to cold environments has been studied
60 for a long time. So-called cold exposure refers to the direct exposure of the human body
61 to an environment lower than normal temperature (20°C). In a cold environment, the
62 human body might can produce a series of physiological reactions, but no definitive
63 conclusion has been reached because this special environment has many influences on
64 the human body, and the individual responses to the cold environment are also different,
65 no definitive conclusion has been reached. Researchers have shown that cold exposure
66 can affect the activities of the nervous[1], cardiovascular[2, 3], musculoskeletal[4, 5],
67 immune[6] and endocrine systems[7]. Cold environments induce long-term effects that
68 increase the risk of cardiovascular disease (CVD) morbidity and mortality[8]. However,
69 no studies have been reported on the effect of cold environments on the development
70 of medial arterial calcification (MAC).

71 The founder of modern medicine, William Osler, once put forward the view of
72 'vascular ageing, a man is as old as his arteries', revealing the important connection
73 between vascular ageing and individual ageing[9]. MAC is an important part of
74 vascular ageing. It is a systemic vascular disease that is distinct from atherosclerosis
75 and is commonly seen in diabetes, end stage renal disease and ageing, resulting in
76 increased vascular stiffness[10, 11], diastolic heart failure[12], impaired coronary
77 perfusion[13] and chronic limb ischaemia[14]. MAC was previously thought to be a
78 simple passive deposition of calcium and phosphorus. However, researchers have paid
79 more attention to the pathogenesis of arterial calcification since the discovery of bone

带格式的: 缩进: 首行缩进: 1 字符

80 morphogenetic protein (BMP) in tissue with MAC[15-19]. Nonetheless, the
81 pathogenesis of MAC has not been fully elucidated – except for the pathogenesis of
82 arterial calcification caused by a single gene mutation, which has been clearly studied
83 – and there is a lack of treatment for the disease.

84 According to MISEV 2018, extracellular vesicles (EVs) can be divided into two
85 subgroups: small EVs (sEVs or exosomes, < 100 nm or < 200 nm) and medium/large
86 EVs (m/IEVs, > 200 nm)[20]. Exosomes are membranous vesicles secreted by cells,
87 usually 50–150 nm in diameter, which are widely present in various body fluids and,
88 carry lipids, proteins, messenger RNAs (mRNAs), microRNAs (miRNAs), non-coding
89 RNAs (ncRNAs) and other important biological function molecules[21-25].
90 Calcification of the major arteries is an important phenotype of vascular ageing.
91 Researchers have found that exosomes play different roles in MAC[26-29]. Thus, we
92 hypothesis Exosomes may serve as communication vesicles and mediate vascular
93 calcification at an ambient temperature.

设置了格式: 非上标/ 下标

94 Autophagy is associated with many physiological and pathological processes, such
95 as development, differentiation, neurodegenerative diseases[30, 31], stress[32],
96 infection[33] and cancer[34]. Mammalian target of rapamycin (RAPA) (mTOR) is an
97 important kinase that regulates the induction of autophagy. Activated mTOR acts via
98 AKT and mitogen-activated protein kinase (MAPK) signalling to inhibit autophagy,
99 while adenosine monophosphate-activated kinase (AMPK) and p53 signalling
100 negatively regulate mTOR to promote autophagy. Studies have shown that autophagy
101 is particularly closely related to ageing[35]. Cell ageing and autophagy have a common
102 regulatory pathway that involves key proteins such as mTOR, SIRT1 and p53. With
103 ageing, cellular senescence is usually accompanied by a decrease in the level of
104 autophagy as well as the degradation of damaged organelles and proteins; the decrease
105 in the level of autophagy can accelerate the ageing process[13, 36]. Multiple studies
106 have shown that autophagy occurs in the context of atherosclerosis[37-39] and
107 hypertension[40]. Evidence suggests that RAPA, an inducer of autophagy, prevents
108 phenotypic switching and the hyperproliferation of vascular smooth muscle cells
109 (VSMCs)[41]. Therefore, autophagy may act as an endogenous protective mechanism
110 to alleviate calcification in VSMCs[42]. These phenomena suggest that autophagy
111 plays a key role in arterial calcification.

112 In the present study, we hypothesised that plasma-derived exosomes isolated from
113 mice subjected to cold temperature exposure (CT-Exo) protect against~~attenuate~~ the
114 calcification and senescence of the aortic media by regulating the level of autophagy.
115 We thoroughly~~deeply~~ explored the effects of CT on the pathogenesis of MAC and
116 clarified its mechanism. ~~We investigated~~ whether cold temperature exposure (CT)
117 can protect against~~attenuate~~ MAC, whether autophagy is involved in arterial
118 calcification during CT and whether plasma-derived exosomes play a protective role
119 by regulating autophagy. Our findings should~~might~~ provide new ideas and new ways
120 to explore the pathogenesis and prevention ~~methods~~ of MAC.

121

122 **Methods and materials**

123

124 Cell Culture

125 VSMCs were purchased from the National Platform of Experimental Cell Resources
126 for SciTech (Beijing, China). They were incubated in Dulbecco's Modified Eagle's
127 Medium (DMEM) (Gibco, Grand Island, NY, USA) with 10% foetal bovine serum
128 (FBS; Gibco) and 1% penicillin-streptomycin (P1400, Solarbio, Beijing, China). The
129 culture medium was refreshed every 3 days and the cells were cultured at 37°C with a
130 humidified atmosphere of 5% CO₂. To induce calcification, VSMCs were cultured in a
131 medium containing 10 mM β-glycerophosphate (β-GP; 50020, Sigma-Aldrich, St.
132 Louis, MO, USA) to induce the osteoblastic differentiation of VSMCs. To reveal the
133 effect of exosomes isolated from mice subjected to room temperature exposure (RT-
134 Exo) or CT-Exo on the osteoblastic differentiation of VSMCs and the mechanism
135 involved, VSMCs were incubated with 200 ng/μL of CT-Exo or RT-Exo in ~~the~~
136 subsequent experiments.

137 To investigate the effect of autophagy on VSMC calcification, cells were pre-treated
138 with 5 mM of the autophagy inhibitor 3-MA (5142-23-4; SelleckChem, USA) or 1
139 μM of the autophagy inducer RAPA (53123-88-9; SelleckChem) for 30 min. The cells
140 were treated with β-GP for various times and then collected for different experiments:
141 after 3 days, cells were collected for western blotting; after 10 days, cells were collected
142 for senescence-associated β-galactosidase (SA-β-gal) staining (C0602; Beyotime
143 Institute of Biotechnology, Shanghai, China); after 14 days, cells were collected for
144 alkaline phosphatase (ALP) activity detection (A059-1-1; Nanjing Jiancheng
145 Bioengineering Institute, Nanjing, China) and ALP staining (Solarbio); and after 28
146 days, cells were collected for ARS staining (G1038; Servicebio, Wuhan, China).

147 Agonists and inhibitors of the AMPK/mTOR signalling pathway were used to
148 investigate its role in calcification. VSMCs were stimulated with 10 μM of Compound
149 C (S7306; SelleckChem) or 10 μM of MHY1485 (S7811; SelleckChem) for 30 min and
150 then treated with 200 ng/μL of CT-Exo for 48 h. p-AMPK, t-AMPK, p-mTOR, t-mTOR
151 and RUNX2 protein expression was evaluated in the cell lysates. The SA-β-gal and
152 ARS staining was the same as described above; CT-Exo, Compound C and MHY1485
153 were changed once every 3 days for a period of 10 or 28 days, respectively.

154 Plasma Collection and Administration

155 ~~Six week old male mice (n = 6) were systemically treated with phosphate buffered~~
156 ~~saline (PBS), CT plasma or CT-Exo^{free} plasma (100 μL/injection) via tail intravenous~~
157 ~~injection 8 times over 24 days[43]. CT plasma was isolated from mice subjected to CT~~
158 ~~for 30 days (4–8°C). Two weeks later, the mice were intraperitoneally injected with~~
159 ~~vitamin D (VD) for 5 days. CT plasma or CT-Exo^{free} plasma was isolated from mice~~
160 ~~subjected to CT for 30 days (4–8°C). CT-Exo^{free} plasma was produced as follows: CT~~
161 ~~plasma was diluted with PBS (1:4, v/v), and then ultracentrifuged at 100,000 g for 18~~
162 ~~h to collect the supernatant. After centrifugation, the exosomes were concentrated at the~~
163 ~~bottom of the test tube and about 80% of the upper plasma had been collected, CT-~~
164 ~~Exo^{free} plasma was filtered by 0.22 μm filter and centrifuged at 4,000 g to approximately~~
165 ~~the initial plasma volume by ultrafiltration in a 15 mL Amicon Ultra-15 centrifugal filter~~
166 ~~unit (Millipore, Billerica, MA, USA). The exosomes were stored at –80°C before use.~~
167

带格式的: 缩进: 首行缩进: 1 字符

168 Six-week-old male mice (n = 6) were systemically treated with phosphate-buffered
169 saline (PBS), CT plasma or CT-Exo^{free} plasma (100 μ L/injection) via tail intravenous
170 injection 8 times over 24 days (From 0 day to 24th day)[43]. On At the 14th day, the mice
171 were intraperitoneally injected with vitamin D (VD) for 5 consecutive days, and mice
172 were sacrificed after waiting for another week of PBS, CT plasma or CT-Exo^{free} plasma
173 treatment.

174 Isolation and Identification Characterisation of Exosomes

175 Plasma samples were obtained from RT mice (kept at 22–25°C) or CT mice (kept at 4–
176 8°C) for 30 days. Briefly, we collected the whole blood of mice using cardiac blood
177 collection technology was collected into Eppendorf (EP) tubes containing Ethylene
178 Diamine Tetra Acetic Acid (EDTA) anticoagulant. Blood samples were processed
179 within 30 min of collection. The mixture was centrifuged to collect the plasma at 3,000
180 g for 20 min. Subsequently, the plasma underwent successive centrifugation at 3,000 g
181 for 20 min and then 10,000 g for 30 min to discard dead cells and cellular debris. Then
182 supernatant was collected, supernatant:PBS=1:4 Plasma+PBS suspension was added to
183 the ultra-high centrifuge tube. The final supernatant was ultracentrifuged at 100,000 g
184 for 120 min. The supernatant was removed, with and leave 500 μ L left at the bottom
185 and then added resuspended 11 mL in PBS was added to resuspend, before being
186 ultracentrifuged again at 100,000 g for 120 min (avoiding freeze-thaw cycles) and then
187 re-suspended in 15 mL of PBS. The suspension was filtered through a 0.22 μ m filter
188 steriliser (Millipore) and centrifuged at 4,000 g to approximately 200 μ L by
189 ultrafiltration in a 15 mL Amicon Ultra-15 centrifugal filter unit (Millipore). All
190 procedures were performed at 4°C. Exosomes were stored at -80°C or used for the
191 downstream experiments.

192
193 The exosomal protein content was quantified with the BCA protein assay kit (P0012;
194 Beyotime). Transmission electron microscopy (TEM; H-7650, Hitachi, Tokyo, Japan)
195 and dynamic light scattering (DLS) with a NanosizerTM instrument (Malvern
196 Instruments, Malvern, UK) were used to observe the morphology and measure the size
197 distribution of exosomes, respectively. The protein expression of exosomal markers
198 (TSG101, CD81 and CD9) was assessed by western blotting.

199 For *in vitro* assays, exosomes in different groups were used at the concentration of
200 200 ng/ μ L. For *in vivo* experiments, exosomes were used at 200 μ g (dissolved in 100
201 μ L PBS for intravenous injection) per time and per mouse.

202 TEM

203 VSMCs were fixed overnight in 2.5% glutaraldehyde and post-fixed in 1% osmic acid
204 for 2 h. The samples were then dehydrated, embedded and sectioned. After being double
205 stained with 3% uranyl acetate and lead nitrate, the autophagic structures in the cells
206 were viewed using a TEM (H-7650, Hitachi, Tokyo, Japan).

207 Exosome Uptake Assay and Tracing

208
209 *In vitro*, CT-Exo were labelled with PKH26 red fluorescent dye (MINI26-1KT, Sigma-
210 Aldrich) according following to the manufacturer's protocol. After removing the unbound
211

带格式的: 缩进: 首行缩进: 2 字符

设置了格式: 上标

设置了格式: 非上标/ 下标

设置了格式: 上标

带格式的: 缩进: 首行缩进: 1 字符

212 dye, CT-Exo were added to the VSMCs and incubated at 37°C for 6 h. After discarding
213 the culture supernatant and washing the cells with PBS, the cells were fixed with 4%
214 paraformaldehyde (PFA) for 15 min and then incubated with DAPI (C0065; Solarbio)
215 to stain the nuclei. The uptake of the red PKH26-labeled CT-Exo by VSMCs was
216 determined with a fluorescence microscope (Nikon Instruments Korea, Seoul, Korea).

217 *In vivo*, to explore whether CT-Exo could be transported from bone to blood vessel
218 walls after intramedullary injection, 100 μ L of 1 μ g/ μ L CT-Exo ~~w~~asere labelled with 5
219 μ L of 200 μ g/mL 1,1'-dioctadecyl-3,3',3'-tetramethylindotricarbocyanine iodide (DiR;
220 2024243, Invitrogen, Carlsbad, CA, USA) ~~accord~~following to the manufacturer's
221 instructions. Then, the same was ultracentrifuged to remove unbound dye. Mice were
222 injected with DiR-labelled CT-Exo via the tail vein injection for 3 consecutive days.
223 Live imaging was performed 24 h after the last injection. The mice were killed, organs
224 ~~were~~ removed for ~~photographing~~imaging, the thoracic aorta of the mice was dissected
225 and immunofluorescence staining was performed on quick frozen sections to analyse
226 the uptake of exosomes in arterial vessels. An anti-TSG101 antibody (1:250, bs-1365R,
227 Bioss, Beijing, China) was used to label exosomes.

228

229 **Measurement of Reactive Oxygen Species (ROS) Generation**

230 Intracellular ROS production was measured by flow cytometry using the cell-
231 permeable fluorogenic probe DCFH-DA (S0033S; Beyotime) according to the
232 manufacturer's instructions. Briefly, calcified VSMCs were treated with 200 ng/ μ L of
233 CT-Exo or PBS for 6 days, washed three times with PBS and then incubated with $1 \times$
234 10^{-5} μ M DCFH-DA at 37°C for 20 min.

235

236 **Apoptosis Assay**

237 VSMCs were treated with CT-Exo or PBS with or without β -GP for 3 days. Apoptosis
238 was measured using the Annexin V-FITC/PI Detection Kit (556547, BD Bioscience,
239 USA) according to the manufacturer's protocol. For Annexin V-FITC/PI staining, the
240 treated cells were harvested, washed twice with PBS and resuspended in 300 μ L of $1 \times$
241 binding buffer, at room temperature in the dark, followed by incubation with 5 μ L of
242 Annexin V-FITC for 15 min and 10 μ L of PI solution for 5 min. Next, the cell
243 suspension was diluted with 200 μ L of annexin V binding buffer and analysed by flow
244 cytometry.

245

246 **Animal Study**

247 Mice were housed in the Animal House of the Second Xiangya Hospital with a 12-h
248 photoperiod. All experiments were started on 7–8 week old mice. Mice were placed in
249 RT (22–25°C) or CT (4–8°C) environments, and their hair changes, mental state and
250 activity were observed. Their body mass was measured and recorded at regular intervals
251 every week. On the 30th day after modelling, blood was taken to measure ALT levels.
252 Mice were shaved to observe whether their skin was frostbitten, important organs were
253 collected for photography and the mass of the heart, liver, spleen, lung, and kidney
254 tissues was measured. The organ indices and lung wet/dry weight of the mice were
255 calculated.

带格式的: 缩进: 首行缩进: 1 字符

设置了格式: 上标

带格式的: 缩进: 首行缩进: 1 字符

Mice were injected intraperitoneally with VD (500 U/g/day) for 5 days to induce arterial calcification and ageing. Mice were fed with regular chow throughout the entire experiments. The RT mice were kept at 22–25°C for 30 days. The CT mice were first kept at 18°C for 7 days (for adaptation), and then kept at 4–8°C for another 30 days. The 4–8°C cold room was equipped with a ventilation system that allowed cold air to circulate.

After 30 days of RT or CT, the mice were administered a high-dose of VD for 5 consecutive days, followed by waiting for 7 days. This treatment occurred at either RT or CT, depending on the initial 30-day treatment. All live mice (n = 6) were sacrificed via the intraperitoneal injection of sodium pentobarbital (50 mg/kg) followed by cervical dislocation. Blood samples were collected to detect the levels of aminotransferase (ALT), using an automatic biochemical analyser (Chemray 800; Redu Life Technology, Shenzhen, China). The thoracic aorta was embedded in paraffin, sectioned and then stained with ARS. The artery from the aortic arch to the iliac branch was isolated for the determination of arterial wall calcium content. No mice died during the experiment.

In another experiment, CT mice were injected intraperitoneally with GW4869 (2 mg/kg; S7609, SelleckChem) to inhibit circulating exosomes[44, 45]. Immunohistochemistry was carried out to determine RUNX2 expression in aortic tissues. ARS staining were used to detect MAC. Finally, the calcium content was measured.

带格式的: 缩进: 首行缩进: 2 字符

The impact of CT-Exo and RT-Exo on acute arterial calcification and the role of miR-320a-3p in the CT-Exo-induced alleviation of arterial calcification were also evaluated. Mice were injected intravenously with 200 µg of CT-Exo, AntagomiR-320a-3p or AntagomiR-NC-pre-treated CT-Exo, or an equal volume of PBS (100 µL per mouse) every 3 days until the end of the experiment (n = 6 per group). At the same time, the mice were injected with VD for 5 consecutive days, followed by waiting for 7 days. Blood samples were collected to detect the levels of blood urea nitrogen (BUN), creatinine (CREA), calcium, and phosphorus using an automatic biochemical analyser. The thoracic aortas were dissected. Immunohistochemistry was carried out to determine the levels of RUNX2 in aortic tissues. ARS or Von Kossa staining (G1043; Servicebio) was used to detect artery calcification. Finally, the calcium content was measured.

带格式的: 缩进: 首行缩进: 1 字符

To explore whether miR-320a-3p was the only effective component in CT-Exo, we intravenously injected 200µg CT-Exo, 5mg/kg AgomiR-320a-3p, 5mg/kg AgomiR NC, or equivalent volume of PBS (100 per mouse) into mice every 3 days until the end of the experiment (n = 6 per group). Meanwhile, mice were continuously injected with VD for 5 days and then waited for 7 days. The thoracic aorta was dissected, ARS staining was performed to detect the content of mineralised nodules in the arteries and calcium content was measured. Immunohistochemical detection of RUNX2 levels was performed on the aortic mesomembrane.

Next, whether CT-Exo exerts an inhibitory effect on MAC *in vivo* through the autophagy pathway was investigated. The mice were randomly divided into six groups (n = 6 per group): PBS (CTRL), VD+PBS (PS), VD+CT-Exo (CT-Exo), VD+3-MA (3-MA), VD+RAPA (RAPA) and VD+CT-Exo+3-MA (CT-Exo+3-MA). Mice were

300 intraperitoneally injected with either 3-MA (15 mg/kg) or RAPA (2mg/kg) starting 5
301 days before the first CT-Exo injection (CT-Exo was injected every 3 days for a total of
302 eight injections) until the experiment was terminated. Then, arterial calcification was
303 induced by VD 2 weeks before the mice were sacrificed. One mouse from the CT-
304 Exo+3-MA group and the RAPA group died from unknown causes after being treated
305 four times. Immunohistochemistry was carried out to determine p21 expression in
306 aortic tissues. MAC was detected by ARS and Von Kossa staining and the calcium
307 content was measured.

308

309 **Quantitative Real-Time Polymerase Chain Reaction (qRT-PCR)**

310 Total RNA was isolated from cells with TRIzol Reagent (Invitrogen) based on the
311 manufacturer's instructions[46]. For miRNA detection, miRNA was reverse transcribed
312 and analysed by TB Green® Premix Ex Taq™ II (Tli RNaseH Plus; RR820A, Takara,
313 Kyoto, Japan) based on the manufacturer's protocol and using U6 as the normalisation
314 control. U6 (HmiRQP9001) and miR-320a-3p (HmiRQP0405) primers were purchased
315 from GeneCopoeia (Guangzhou, China).

316

317 **RNA Sequencing**

318 The RT-Exo and CT-Exo groups were selected for RNA sequencing (n = 3 per group).
319 Total RNA was extracted and quantified using a NanoDrop spectrophotometer and an
320 Agilent 2100 bioanalyzer (Agilent, Santa Clara, CA, USA). A messenger RNA (mRNA)
321 library was then constructed and amplified with Phi29 to produce 100 base pair reads
322 on the BGISEQ500 platform (BGI, Shenzhen, China). SOAPnuke (V1.5.2) was used to
323 filter the sequencing data, and Bowtie2 (V2.2.5) was used to compare the clean reads
324 with the gene database established by Shenzhen Beijing Genomics Institute to calculate
325 gene expression levels and identify differentially expressed genes (DEGs) (fold-change >
326 1.5, $q < 0.05$). The annotated DEGs were analysed using Phyper- based on Gene
327 Ontology (GO) and Kyoto Encyclopedia of Genes and Genomes (KEGG) analysis.
328 Gene set enrichment analysis (GSEA) was used to evaluate DEGs enriched for either
329 negatively or positively correlated genes.

330

331 **RNA Interference**

332 Small interfering RNAs (siRNAs) and the negative control RNA duplex (siRNA-NC)
333 were purchased from GenePharma Biotech (Shanghai, China). The miR-320a-3p
334 mimics or miR-320a-3p inhibitor and scrambled oligonucleotides (mimics NC or
335 inhibitor-NC) were purchased from GenePharma Biotech. These were transfected into
336 cells during the logarithmic growth phase. The transfection was performed using the
337 GP-transfect-Mate transfection reagent (GenePharma Biotech) according to the
338 manufacturer's protocol. The transfected sequences of the miR-320a-3p
339 mimics/inhibitor and siRNA oligonucleotides are shown in Additional file 1, Table S1.

340 AgomiRs or AntagomiRs were purchased from GenePharma Biotech. CT-Exo were
341 transfected with AntagomiR-320a-3p or AntagomiR-NC at 200 nM for 60 min at 37°C.
342 The AgomiRs and AntagomiRs that were not transfected were removed by
343 centrifugation at 4,000 g for 5 min using a 100 kDa Amicon Ultra-4 Centrifugal Filter

带格式的: 缩进: 首行缩进: 0 字符

带格式的: 缩进: 首行缩进: 0 字符

344 Unit (Millipore)[26]. The internalisation of AntagomiR-NC-Cy3 by CT-Exo was
345 assessed by qRT-PCR. Treatment with CT-Exo and other AntagomiRs was used for
346 subsequent experiments.

347

348 **Western Blotting**

349 Total protein was extracted from cultured VSMCs, artery samples or exosomes with
350 radioimmunoprecipitation assay (RIPA) buffer (P0013B; Beyotime). The protein
351 concentration was measured by the BCA assay. Total protein (20–40 µg) was submitted
352 to 8–12% sodium dodecyl sul~~phate~~-polyacrylamide gel electrophoresis (SDS-PAGE)
353 for separation. The separated protein was transferred onto 0.2 or 0.45 µm
354 polyvinylidene difluoride (PVDF) membranes (Millipore). The membranes were
355 incubated in 5% non-fat milk or bovine serum albumin (BSA) (depending on the
356 primary antibody), followed by incubation overnight with primary antibody. The
357 following primary antibodies were used: anti-CD9 (ab92726, Abcam, 1:2000), anti-
358 CD81 (ab109201, Abcam, 1:1000), anti-TSG101 (bs-1365R, Bioss, 1:500), anti-
359 RUNX2 (ab76956, Abcam, 1:1000), anti-BMP2 (bs-10696R, Bioss, 1:500), anti-p53
360 (10442-1-AP, Proteintech, 1:3000), anti-p62 (18420-1-AP, Proteintech, 1:2000), anti-
361 ATG5 (66744-1-Ig, Proteintech, 1:4000), anti-LC3B (14600-1-AP, Proteintech, 1:4000,
362 to determine the LC3B-II:LC3B-I ratio), anti-PDCD4 (12587-1-AP, Proteintech,
363 1:1000), anti-p-AMPK (sc33524, Santa Cruz, 1:500), anti-t-AMPK (sc25792, Santa
364 Cruz, 1:500), anti-p-mTOR (2971, CST, 1:1000), anti-t-mTOR (2983, CST, 1:1000),
365 anti-β-actin (20536-1-AP, Proteintech, 1:3000) and anti-GAPDH (10494-1-AP,
366 Proteintech, 1:5000). After washing the blots, they were incubated in secondary
367 antibody conjugated to horseradish peroxidase (SA00001-1 or SA00001-2, Proteintech,
368 1:5000) for 1 h at room temperature. The immunoreactive bands were ~~visualized~~
369 ~~visualised~~ with chemiluminescent assay using a chemiluminescence kit (RPN2232,
370 Amersham Biosciences Ltd., UK) and then analysed with an Amersham Imager 600
371 (General Electric, USA) and Image-Pro Plus software (version 6.0). The relative protein
372 expression level was normalised to the intensity of the β-actin or GAPDH band.

373

374 **Luciferase Reporter Assay**

375 For the luciferase reporter assay, VSMCs were co-transfected with a luciferase reporter
376 carrying the wild-type PDCD4 3'-untranslated region (UTR), a mutant PDCD4 3'-UTR
377 and miR-320a-3p mimics or scramble oligonucleotides. Forty-eight hours after
378 transfection, luciferase activity was quantified with the luciferase assay system
379 (Promega, Madison, WI, USA). The nucleotide sequences of primers for the
380 construction and mutation of 3' UTR PDCD4 mRNA were purchased from Ribobio
381 (Guangzhou, China).

382

383 **Immunohistochemistry**

384 As mentioned above, the expression of RUNX2 and p21 in aortic tissue was examined
385 by immunohistochemistry[45]. In brief, arterial tissue sections were incubated at 65°C
386 for 2 h, dewaxed in turpentine twice for 10 min each; and rehydrated in 99%, 85% and
387 75% ethanol for 5 min each. Antigen retrieval was performed in a trypsin-EDTA

388 solution. Next, sections were blocked with 5% BSA for 30 min at room temperature
389 and incubated with specific primary antibodies, including anti-RUNX2 (bs-1134R,
390 Bioss, 1:300) and anti-21 (10355-1-AP, Proteintech, 1:400) at 4°C overnight. The
391 following day, sections were incubated with the appropriate secondary antibody
392 conjugated to horseradish peroxidase (PV-9000, ZSGB-BIO, Beijing, China) at room
393 temperature for 30 min. For control experiments, the primary antibody was replaced by
394 PBS. Finally, the sections were incubated with DAB chromogenic solution (DA1015;
395 Solarbio) for 1 min at room temperature. Nuclei were counterstained with haematoxylin
396 (Solarbio) for 1 min at room temperature. The stained tissue was observed under a
397 CX31 light microscope (Olympus Corporation, Japan). Images were taken at 100×
398 magnification and ~~analysed~~ images analysed using Image-Pro Plus software (version
399 6.0).

400

401 **Analysis of Vascular Calcium Content**

402 Arterial samples were decalcified with 0.6 N HCl at 4°C for 48 h. After determining
403 the protein concentration, the calcium content in the supernatant was assessed using a
404 commercial kit (C004-2-1; Nanjing Jiancheng Bioengineering Institute). The vascular
405 calcium content was normalised to the protein concentration.

406

407 **Statistical Analysis**

408 All data are presented as the mean ± standard deviation of three independent
409 experiments. Data were analysed and plotted using GraphPad Prism software (San
410 Diego, CA, USA) and ImageJ software (National Institutes of Health, Bethesda, MD,
411 USA). The unpaired, two-tailed Student's *t*-test was conducted to compare two groups.
412 One- or two-way analysis of variance (ANOVA) with the Bonferroni *post hoc* test was
413 used to compare three or more groups. Results were considered significant when the *p*-
414 value was < 0.05. In the Figures, statistical significance is indicated as ns > 0.05; **p* <
415 0.05; ***p* < 0.01; ****p* < 0.001 and *****p* < 0.0001.

416

417 **Results**

418 **CT-Exo Played a Certain Role in the Progression of Protected against VD-Induced 419 **MAC in CT Mice****

420 Firstly, we tested the food intake and body weight of mice in the low-temperature model,
421 and the results showed that compared with the RT group, the average food intake of
422 mice in the CT group was significantly increased, indicating that low-temperature can
423 increase the food intake level of mice. The measurement of the weight of mice indicated
424 that the weight of CT group mice showed a decreasing trend within 6 days, and
425 gradually recovered and increased after 6 days. We observed that over time, the overall
426 body weight was attenuated despite the stable food intake in CT mice (Additional file 1:
427 Fig. s1, a and b). The level of ALT showed no significant difference between these two
428 groups (Additional file 1: Fig. s1c). After shaving the hair of the mice (Additional file 1:
429 Fig. s2a), we found that the mice showed no signs of numbness or frostbite, and there
430 wasere no erythema, edema, hard gangrene, infarction, or epidermal detachment on the
431 skin surface. After dissecting the mice, the liver, lungs, spleen, heart, and kidneys were

设置了格式: 字体颜色: 深红

设置了格式: 字体颜色: 深红

432 taken. The general morphology is shown in [Additional file 1: Fig. s2b](#). The organ index
433 can objectively reflect the function of relevant organs and is one of the important
434 biological indicators for experimental animals. As shown in [Additional file 1: Fig. s2c](#),
435 except for the increase in cardiac index in the CT group, there was no significant
436 difference in liver, spleen, lung, kidney organ indices and liver morphology
437 (Additional file 1: Fig. s2d) between two group mice, suggesting that all CT and RT
438 mice are in a healthy metabolic status. H&E staining of lung tissues showed that
439 exposure to cold stress slightly aggravated lung damage. In the lung slightly disruption
440 of the alveolar structure, as well as vascular base thickening, a mild thickened alveolar
441 wall and minimal inflammatory cell infiltration, were observed when compared to the
442 RT group (Additional file 1: Fig. s2d). The CT mice had higher lung interstitial
443 inflammation score and lung wet/dry ratio compared with the RT mice, but only by
444 trend (Additional file 1: Fig. s2, e and f).

设置了格式: 字体颜色: 深红

设置了格式: 字体颜色: 深红

设置了格式: 字体颜色: 深红

设置了格式: 字体颜色: 深红

445 To investigate the protective effect of CT on MAC, we subjected mice to CT or RT
446 for 30 days and then injected with VD to induce MAC. We kept mice in the CT or RT
447 environment throughout the experiment (Fig. 1a). Based on ARS staining of the
448 thoracic aorta, there was a lower degree of MAC in CT mice compared with RT mice
449 (Fig. 1, b and c). The MAC in cold-exposed mice was significantly blunted, as
450 evidenced by the decreased calcium content (Fig. 1d). The effect of a cold environment
451 on the body's metabolism is holistic and systemic. We wondered whether these anti-
452 arterial calcification protective effects of CT on MAC in mice could be transferred
453 through circulating blood factors. We collected plasma from CT mice and then
454 intravenously injected mice with MAC with CT-Exo or CT-Exo^{free} plasma every 3 days
455 for a total of eight times (Fig. 1e). Surprisingly, the CT-Exo group had the lowest ARS-
456 positive area of all mice with MAC. Treatment with CT-Exo^{free} plasma slightly
457 ameliorated the degree of MAC, as shown by the ARS staining and calcium content.
458 However, the effect of CT-Exo^{free} plasma was much lower CT-Exo plasma, which might
459 suggest that exosomes-CT-Exo play an important role in preventing the calcification
460 formation anti-MAC effect (Fig. 1, f to h). Subsequently, we explored the role of CT-
461 Exo in CT mice with MAC. We intraperitoneally injected the mice with the exosome
462 inhibitor GW4869, which blocks exosome production, every other day (Fig. 1i). The
463 ARS staining area, RUNX2 expression and arterial calcium and calcification were
464 significantly lower in CT mice compared with CT+GW4869 mice (Fig. 1, j to n),
465 suggesting that GW4869 reverse the protective effects of CT accelerated MAC under
466 CT. These results indicate that inhibition of endogenous CT-Exo can promote MAC. ▲

带格式的: 缩进: 首行缩进: 1 字符

设置了格式: 字体: (中文) 宋体

467 **CT-Exo Mediated the CT-Induced MAC Inhibitory Effects in Mice**

468 To directly identify the effects of exosomes, we subjected the mice to RT or CT for 30
469 days, isolated exosomes from them (RT-Exo or CT-Exo) and purified them by hyper-
470 centrifugation ([Additional file 1: Fig. s3a](#)). As viewed with TEM, CT-Exo
471 and RT-Exo exhibited a cup-like morphology ([Additional file 1: Fig. s3b](#)).
472 Nanoparticle tracking analysis (NTA) revealed that CT-Exo and RT-Exo had mean
473 diameters of 110.7 ± 39.6 and 109.6 ± 40.9 nm, respectively ([Additional file 1: Fig.](#)
474 [s3c](#)), which are similar to a previous report[47]. Western blotting showed that a vast

476 majority of the isolated CT-Exo and RT-Exo expressed exosomal markers including
477 TSG101, CD9 and CD81 (Additional file 1: Fig. s3d), which further indicates that these
478 vesicles are exosomes. To determine whether exosomes could be incorporated by aortic
479 VSMCs *in vivo*, we injected DiI-labelled CT-Exo into mice via the tail vein and tracked
480 their distribution. We adjusted the fluorescence intensity of control mice to exclude the
481 interference of autofluorescence. We successfully injected the DiI-labelled CT-Exo
482 into the mice through the tail vein (Fig. 2a). Mice photography mainly detected the
483 fluorescence signal in the liver and spleen (Additional file 1: Fig. s4). Considering that
484 the relatively stronger fluorescence signal of the liver and spleen masked the
485 fluorescence signals of other organs, we removed the liver and spleen, then repeated
486 the imaging. Photographs showed that the fluorescent signals of the DiI-labeled
487 exosomes entered the aorta after injection *in vivo*. The fluorescence was mainly
488 distributed in the aorta (Fig. 2a). In addition, CT-Exo injection significantly increased
489 the expression of the exosomal marker TSG101 in VSMCs in the aortic media
490 (Additional file 1: Fig. s5). Moreover, TSG101 colocalised with alpha smooth muscle
491 actin (α -SMA), which suggests that VSMCs could take up the exosomes. Hence, we
492 successfully injected exogenous CT-Exo into mice and they were then taken up by
493 VSMCs in the aorta.

设置了格式: 字体: 倾斜

494 To investigate whether CT-Exo protect VSMCs against arterial calcification *in vivo*,
495 we analysed the calcification level by using an *in vivo* model of VD-induced MAC in
496 mice (Fig. 2b). VD-induced mice developed significant MAC compared with the
497 vehicle control (PBS). Intriguingly, the MAC level in CT-Exo-treated mice ranged from
498 undetectable to just very low, as demonstrated with the ARS (Fig. 2, c and f) and Von
499 Kossa staining (Fig. 2, d and h). At the same time, based on the staining results, RT-
500 Exo treatment slightly weakened MAC compared with PBS treatment. Unfortunately,
501 there was ~~not a~~ significant inhibition of MAC in the RT-Exo group compared with the
502 PBS group (Fig. 2, c to h). Moreover, the aortic calcium content (Fig. 2g) and RUNX2
503 immunostaining (Fig. 2, e and i) were significantly decreased in CT-Exo-treated mice
504 compared with the VD-treated and RT-Exo-treated mice. These results show that CT-
505 Exo serve as a protective factor in VD-induced MAC in mice.

带格式的: 缩进: 首行缩进: 1 字符

506

507 **CT-Exo Prevented Osteogenic Differentiation and Senescence of VSMCs via** 508 **Autophagy**

509 To determine whether CT-Exo play a vital effect on the osteogenic differentiation and
510 senescence of VSMCs, we examined whether these exosomes could be taken up by
511 VSMCs. We labelled CT-Exo with PKH26 and incubated VSMCs with the labelled
512 exosomes. Fluorescence microscopy analysis showed that the labelled exosomes were
513 taken up by the VSMCs (Fig. 3a). It is widely believed that the process of MAC is
514 similar to bone mineralisation. ALP, RUNX2 and mineralised matrix are recognized
515 phenotypic markers of osteoblasts and are upregulated during osteoblast differentiation
516 of VSMCs[16, 47]. Consistent with our previous results, CT-Exo treatment
517 significantly protected VSMCs against~~inhibited~~ β -GP-induced osteogenic conversion
518 ~~of VSMCs~~, as demonstrated by the remarkably reduced ARS (Fig. 3, b and c) and ALP
519 (Fig. 3f) staining of β -GP-treated VSMCs, and markedly decreased ALP activity (Fig.

3g) and the expression of RUNX2 protein (Fig. 3, h and i). VSMCs senescence ~~was~~ ~~were~~ also decreased, denoted by reduced p53 expression (Fig. 3, h and i) and fewer SA-β-gal-positive VSMCs (Fig. 3, d and e). Thus, we verified that CT-Exo could protected VSMCs against ~~attenuated VSMC~~ osteogenic differentiation and senescence *in vitro*.

To investigate the mechanism of anti-calcification protective effect of CT-Exo, we first examined the effect of CT-Exo on autophagosome formation in VSMCs. CT-Exo increased LC3B protein expression and reduced p62 protein expression during the osteoblastic differentiation of VSMCs (Fig. 3, j and k). TEM of typical autophagic structures provided direct evidence to support the CT-Exo-mediated increase in autophagy: there were more autophagosomes in VSMCs treated with CT-Exo than in the negative and positive controls (β-GP treatment alone and PS, respectively) (Fig. 3l). Studies have shown that autophagy plays an important role in the function of VSMCs and the development of vascular diseases, suggesting that autophagy may be a potential target to prevent vascular calcification[48]. It has previously been reported that activating the AMPK[49] and mTOR signalling pathway regulates autophagy directly and indirectly[50]. AMPK could initiate autophagy either by directly phosphorylating the serine/threonine kinase ULK1[51] or indirectly by deactivating mTORC1[52]. As shown in ~~Additional file~~ Additional file 1: Fig. ~~s6a2a~~, exposure to β-GP triggered a significant elevation in ROS production in VSMCs, as revealed by the increase in the percentage of cells with green fluorescence compared with CT-Exo, suggesting that ROS-induced oxidative injury may be involved in CT-Exo-attenuated cell death. As evidenced by Annexin V-FITC/PI double staining with flow cytometry, CT-Exo treatment decreased the percentages of early apoptotic (Annexin V-FITC positive/PI negative) and late apoptotic/dead (Annexin V-FITC/PI double positive) VSMCs (~~Additional file~~ Additional file 1: Fig. ~~s62b~~), revealing the CT-Exo protected VSMCs from apoptosis. Taken together, these data suggest that ~~CT-Exo enhances autophagy during osteoblastic differentiation of VSMCs~~ CT-Exo prevented osteogenic differentiation and senescence of VSMCs via autophagy.

The Autophagy Inhibitor 3-MA Significantly Weakened the Pro-Autophagy Effect of CT-Exo

We next addressed the potential role of autophagy in the osteoblastic differentiation of VSMCs. RAPA, a pharmacological inducer of autophagy, can activate autophagy, cell proliferation and other cellular activities by inhibiting mTOR activity. RAPA treatment suppressed calcification and senescence of VSMCs, as demonstrated by the reduced matrix mineralisation (Fig. 4, a and b), SA-β-gal staining (Fig. 4, c and d) and ALP staining and activity (~~Additional file~~ Additional file 1: Fig. ~~s7~~, a and b) compared with the PS group. We used 3-MA, a pharmacological inhibitor of autophagy, to decrease autophagy during osteoblastic differentiation of VSMCs. 3-MA treatment augmented matrix mineralisation (Fig. 4a, b), SA-β-gal staining (Fig. 4, c and d) and ALP staining and activity (~~Additional file~~ Additional file 1: Fig. ~~s3s7~~, a and b) in VSMCs compared with the PS group. CT-Exo robustly protected VSMCs against ~~alleviated the senescence and~~ osteoblastic differentiation and senescence of VSMCs, similar to RAPA, and the

带格式的: 缩进: 首行缩进: 1 字符

设置了格式: 字体: 非加粗

564 ~~protective~~~~the inhibitory~~ effect of CT-Exo could be ~~reversed~~~~counteracted~~ by 3-MA
565 (Fig. 4, a to d and ~~Additional file~~~~Additional file~~ 1: Fig. s73, a and b).

566 In the mouse model of MAC (Fig. 4e), CT-Exo ~~protected against~~~~attenuated~~ VD-
567 induced MAC. RAPA treatment suppressed MAC and senescence of the aortic media
568 compared with the PS group, as demonstrated by the reduced Von Kossa staining (Fig.
569 4f), p21 expression (Fig. 4h), ARS staining (~~Additional file~~~~Additional file~~ 1: Fig. s73, c
570 and d) and calcium content (~~Additional file~~~~Additional file~~ 1: Fig. s73e). Arterial
571 calcification increased significantly in the group treated with 3-MA plus CT-Exo
572 compared with the CT-Exo-treated group, demonstrated by the increased ARS
573 (~~Additional file~~~~Additional file~~ 1: Fig. s73, c and d) and Von Kossa (Fig. 4, f and g)
574 staining, the elevated calcium content (~~Additional file~~~~Additional file~~ 1: Fig. s73e) and
575 the upregulation of p21 expression (Fig. 4, h and i) compared with the CT-Exo-treated
576 group. Collectively, these results indicate that CT-Exo ~~protects VSMCs against~~~~inhibits~~
577 the osteoblastic differentiation ~~of VSMCs~~ and arterial calcification by promoting
578 autophagy. 3-MA ~~reversed the protective~~~~enhanced the inhibitory~~ effect of CT-Exo on
579 the osteoblastic differentiation of VSMCs. Thus, both *in vitro* and *in vivo*, the
580 ~~protective~~~~inhibitory~~ effect of CT-Exo ~~on~~ ~~against~~ calcification was attenuated by
581 blocking CT-Exo-induced autophagy.

582 To understand the role of the AMPK/mTOR signalling pathway in the induction of
583 autophagy by CT-Exo, we pre-treated VSMCs with CT-Exo for 30 min before β -GP
584 treatment. Western blotting showed that compared with treatment with CT-Exo alone,
585 treatment with 3-MA significantly attenuated CT-Exo-induced autophagy, reflected by
586 the dramatic decrease in p/t-AMPK expression (~~Additional file~~~~Additional file~~ 1: Fig.
587 s73, f and g), whereas p/t-mTOR expression increased significantly (~~Additional~~
588 ~~file~~~~Additional file~~ 1: Fig. s73, f and g). Interestingly, VSMCs were treated with or
589 without CT-Exo or Compound C, an inhibitor of AMPK, or MHY1485, an activator of
590 mTOR. In the presence of Compound C, the CT-Exo-induced inhibition of RUNX2
591 protein expression (~~Additional file~~~~Additional file~~ 1: Fig. s8, a and b), ARS staining
592 (~~Additional file~~~~Additional file~~ 1: Fig. s8, c and e) and SA- β -gal staining (~~Additional~~
593 ~~file~~~~Additional file~~ 1: Fig. s8, d and f) were abolished. Similarly, MHY1485 mimicked
594 the effects of Compound C. Thus, these experiments demonstrate that CT-Exo inhibited
595 osteoblastic differentiation/ageing of VSMCs via the AMPK/mTOR signalling pathway.

596
597 **miR-320a-3p ~~Is~~ was Enriched in CT-Exo and Responsible for the CT-Exo-Induced**
598 **~~protection VSMCs against~~ ~~Reduction in VSMC~~ Calcification/Ageing**

599 To explore the mechanism involved in the CT-Exo-induced ~~protection against~~ -MAC,
600 we employed an Agilent miRNA array to compare the miRNA expression profiles of
601 CT-Exo and RT-Exo from mouse plasma. We identified a total of 1380 miRNAs, of
602 which 71 were differentially expressed (absolute fold-change ≥ 1.5 , $p < 0.05$) between
603 CT-Exo and RT-Exo. We found that 33 miRNAs were much higher and 38 miRNAs
604 were much lower in CT-Exo compared with RT-Exo (Fig. 5a). We selected miR-320a-
605 3p, which was the most abundant miRNA in CT-Exo compared with RT-Exo (Fig. 5**a**).
606 With qRT-PCR, we assessed the changes in miR-320a-3p expression in exosomes from
607 plasma obtained from CT and RT mice. As shown in Fig. 5b, miR-320a-3p expression

带格式的: 缩进: 首行缩进: 1 字符

设置了格式: 字体: 非加粗

608 was higher in CT-Exo. Moreover, miR-320a-3p expression was significantly increased
609 in vessels from CT mice compared with vessels from RT mice (Fig. 5c). After
610 transfection with miR-320a-3p mimics, miR-320a-3p expression in VSMCs was
611 significantly higher than in VSMCs transfected with NC mimics, and miR-320a-3p
612 expression in VSMCs treated with miR-320a-3p inhibitor was significantly lower than
613 in VSMCs treated with the NC inhibitor (Fig. 5d). Moreover, miR-320a-3p
614 overexpression with mimics greatly decreased ALP activity, while miR-320a-3p
615 knockdown with an inhibitor greatly increased ALP activity (Fig. 5e).

616 Previous studies have shown that miR-320a has a certain correlation with the
617 occurrence and development of atherosclerosis[53]. However, the role of miR-320a-3p
618 in VSMCs calcification is largely unknown. To assess the effects of miR-320a-3p on
619 the osteoblastic differentiation of VSMCs, we first determined the effects of miR-320a-
620 3p overexpression or knockdown in β -GP-induced VSMCs. miR-320a-3p
621 overexpression reduced the expression of RUNX2, BMP2 and p21 and increased the
622 expression of LC3B and ATG5 (Fig. 5, f and g). In contrast, miR-320a-3p knockdown
623 inhibited the level of autophagy and promoted VSMCs calcification. We then used
624 specific AntagomiRs to silence miR-320a-3p in CT-Exo. After transfection with
625 AntagomiR-320a-3p, miR-320a-3p expression in CT-Exo decreased significantly (Fig.
626 5h). ARS staining showed VSMCs treated with AntagomiR-320a-3p and CT-Exo
627 induced a much higher extent of mineralised nodule formation than VSMCs treated
628 with AntagomiR-NC and CT-Exo (Fig. 5, i and j). Knocking down miR-320a-3p in CT-
629 Exo significantly reduced the ability of CT-Exo to restrain ALP activity (Fig. 5l) and
630 ALP staining (Fig. 5k). Similarly, VSMCs treated with AntagomiR-320a-3p and CT-
631 Exo showed accelerated senescence of VSMCs compared with VSMCs treated with
632 AntagomiR-NC and CT-Exo (Fig. 5, m and n).

633 We assessed the role of miR-320a-3p in the CT-Exo-induced protection VSMCs
634 against amelioration of MAC in mice subjected to VD treatment (Fig. 6a). ARS staining
635 indicated that ARS-positive mineralised nodule area was markedly elevated in the CT-
636 Exo+AntagomiR-320a-3p group compared with the CT-Exo+AntagomiR-NC group
637 (Fig. 6, b and c). The vascular calcium content analysis confirmed that CT-Exo
638 markedly increased the vascular calcium content after pre-treatment with AntagomiR-
639 320a-3p (Fig. 6d). These findings indicate that miR-320a-3p acts as the mediator of the
640 CT-Exo-induced protection VSMCs against amelioration of calcification of VSMCs.
641 The CT-Exo+AntagomiR-320a-3p mice had slightly higher serum levels of BUN and
642 CREA compared with the CT-Exo mice. Subsequently, both calcium and phosphorus
643 could also be detected in CT-Exo+AntagomiR-320a-3p and CT-Exo mice, but these
644 indicators were not significantly different between the three groups (Fig. 6, e to h).
645 Interestingly, from the expression results of ARS staining (Fig. 6, j and k), calcium
646 content (Fig. 6l) and RUNX2 expression (Fig. 6, m and n), we found that tail vein
647 injection of AgomiR-320a-3p can provide a certain protective effect on arterial media
648 calcification (Fig. 6i), but its protective effect is not as good as that of the CT-Exo group,
649 indicating that miR-320a-3p was the main miRNA in CT-Exo, but not the only active
650 component of CT-Exo.

651

miR-320a-3p ~~Protected~~ ~~Restrained~~ VSMCs ~~Against~~ Calcification and Ageing by Targeting Programmed Cell Death 4 (PDCD4)

To understand the mechanism by which miR-320a-3p restrained VSMCs calcification, we used the online bioinformatics tool TargetScan (Version 7.2, http://www.targetscan.org/vert_72/) and miRDB (<http://mirdb.org/mirdb/index.html>) and miRWalk (<https://http://mirwalk.umm.uni-heidelberg.de/>) to predict potential target genes of miR-320a-3p (Fig. 7a). Among them, PDCD4 is an important tumour suppressor that inhibits carcinogenesis, tumour progression and invasion by inhibiting translation[54]. Recent studies have found that PDCD4 negatively regulates autophagy by inhibiting the expression of ATG5 in tumour cells[55] and plays a certain role in autophagy in the treatment of atherosclerosis[56]. The sequence alignment results illustrated that miR-320a-3p has a complementary pairing relationship with the 3'-UTR region of PDCD4 (Fig. 7b), indicating that PDCD4 may be a target gene of miR-320a-3p. A luciferase reporter assay also demonstrated that miR-320a-3p overexpression reduced the activity of wild type PDCD4 promoter but not mutant PDCD4 promoter (Fig. 7c). In addition, western blotting showed that PDCD4 protein was downregulated by miR-320a-3p mimics and upregulated by miR-320a-3p inhibitor (Fig. 7, d and f). These data suggest that PDCD4 may be a target of miR-320a-3p in VSMCs.

To determine whether PDCD4 mediates the inhibitory effect of miR-320a-3p on VSMC calcification, we also used PDCD4-specific siRNA to block its expression. Western blot detected that all three siPDCD4 sequences could suppress > 70% of PDCD4 protein expression; the third siRNA sequence was the most effective (Fig. 7, e and g). Hence, we used this siRNA in subsequent experiments. PDCD4 downregulation reduced the expression of RUNX2 and p53 (Fig. 7, h and i) and decreased ARS (Fig. 7, j and l) and SA- β -gal (Fig. 7, k and m) staining, indicating that PDCD4 plays a crucial role in VSMC autophagy and calcification. Notably, miR-320a-3p inhibitor enhanced the ARS and SA- β -gal stained areas, but these effects were abolished by ~~the~~ suppression of PDCD4 (Fig. 7, j to m). After silencing PDCD4 by siRNA and inducing calcification, we measured ~~and~~ the expression levels of autophagy-related and phosphorylated proteins in VSMCs 3 days later. Silencing PDCD4 could promote the occurrence of autophagy in VSMCs through the AMPK/mTOR signalling pathway, which was reflected in the overexpression levels of LC3B and ATG5 proteins (~~Additional file~~ ~~Additional file~~ 1: Fig. ~~s~~9, a and b). Taken together, these results demonstrate that miR-320a-3p ~~protected VSMCs against~~ ~~inhibits~~ ~~VSMC~~ calcification by targeting PDCD4.

Discussion

In the present study, autophagy played a vital endogenous protective role during cold exposure under β -GP/VD induction to attenuate MAC. Furthermore, miR-320a-3p, enriched in CT-Exo, promoted autophagy and mediated the ~~protection VSMCs against~~ ~~attenuation of~~ MAC. Meanwhile, PDCD4 is a target gene of miR-320a-3p that regulates autophagy to reduce MAC.

The importance of ambient temperature on mouse physiology is not limited to the context of metabolic disease. Previous studies have shown that ambient temperature

带格式的: 缩进: 首行缩进: 1 字符

带格式的: 缩进: 首行缩进: 1 字符

696 has a profound effect on the physiological responses of mice to infection, tumours and
697 ageing. For example, mice exposed to higher temperatures have better immunity to
698 bacterial, viral and protozoal infections[57, 58]. Mice raised in thermoneutrality have
699 much smaller tumours[59]. Hypothermia correlates with a longer lifespan[60]. Cold
700 exposure has been reported to suppress obesity, insulin resistance, adipose dysfunction
701 and dyslipidaemia by promoting adipocyte thermogenesis[7]. The effects of cold
702 exposure on atherosclerosis are still under debate. Cold exposure prevents
703 atherosclerosis by activating fat thermogenesis, suppressing vascular inflammation and
704 improving dyslipidaemia[61, 62]. In contrast, thermoneutral conditions (30°C) increase
705 vascular inflammation and atherosclerosis by inhibiting adipose thermogenesis[63].
706 Dong et al.[2] found that cold exposure promoted atherosclerotic plaque growth and
707 instability in mice reared at 4°C ~~with~~ cold exposure for 3 or 7 weeks. However, another
708 study showed that long-term cold exposure to 16°C for 8 weeks protected against
709 Western diet–induced atherosclerosis[64]. These contradictory findings may be due to
710 the different cold exposure conditions. Chen et al.[65] showed an inverse J-shaped
711 association between human cardiovascular mortality and ambient temperature,
712 suggesting that moderate cold (ranging from -1.4 ~~to~~ -22.8°C) leads to the lowest risk
713 of cardiovascular death, but both extreme cold (-6.4 ~~to~~ -1.4°C) and heat (29.0 ~~to~~
714 31.6°C) increase cardiovascular death risk. Seki et al.[4] exposed mice to 4°C and found
715 that cold-activated brown fat can ‘freeze’ cancer cells to death. Based on the available
716 research on the effect of cold stimulation on metabolism (insulin resistance, obesity,
717 diabetes, etc.), we found that most researchers used the temperature of 4°C[66, 67].

718 Prior to our study, the effect of cold exposure on MAC had not yet been studied;
719 hence, our exploration of hypothermia and MAC is both novel and very necessary.
720 When designing *in vivo* experimental cold exposure studies in mice, it is important to
721 consider the different metabolic, cardiovascular and heat-sensing responses evoked by
722 different cold stimulation temperatures. Indeed, the lack of standardisation in defining
723 the extent of cold exposure has posed serious challenges in the field. We chose 4–8°C
724 for 30 days to represent relatively chronic stimulation of low temperature in mice.
725 Vascular ageing is manifested by morphological abnormalities of cells and
726 histologically manifested as ~~the~~ increased deposition of collagen fibres, increased and
727 disordered elastic fibres, arteriosclerosis and calcification[68]. We found that
728 MAC/senescence can be weakened in mice subjected to chronic cold stimulation,
729 mainly through CT-Exo, as demonstrated by the significantly increased calcification
730 area of Von Kossa and ARS staining and calcium content as well as ~~the~~ upregulated
731 expression of calcification and ageing marker proteins (RUNX2 and p21). *In vitro*, CT-
732 Exo decreased SA-β-gal staining, ALP activity, RUNX2 and p53 expression and
733 mineralised nodule formation in β-GP-induced VSMCs.

734 Here, using *in vitro* and *in vivo* models of arterial calcification, we found that
735 autophagy plays a vital endogenous protective role during the osteoblastic
736 differentiation of VSMCs. CT-Exo directly potentiated autophagy, which attenuated the
737 osteoblastic differentiation of VSMCs *in vitro* and arterial calcification *in vivo*.
738 Moreover, CT-Exo increased the number of autophagosomes in β-GP-induced VSMCs,
739 increased the expression of the autophagy-related protein LC3B and decreased the

740 expression of p62. The inhibition of autophagy by 3-MA significantly attenuated the
741 inhibitory effect of CT-Exo on the osteoblastic differentiation of VSMCs. In contrast,
742 the promotion of autophagy by RAPA attenuated the osteogenic differentiation of
743 VSMCs. CT-Exo also attenuated arterial calcification by promoting autophagy in mice,
744 as demonstrated by the fact that RAPA but not 3-MA blocked the effect of CT-Exo.
745 Thus, targeting the autophagic pathway may help to prevent or treat vascular
746 calcification[42, 69], ~~which and this~~ provides a theoretical basis ~~for by which~~ CT-Exo
747 ~~to protect against~~attenuate vascular calcification.

748 Intracellular mTOR includes two complexes, mTORC1 and mTORC2. mTORC1
749 regulates cellular protein synthesis and cell growth through phosphorylation and
750 activation of downstream target proteins such as p70 ribosomal S6 kinase 1 (S6K1),
751 while mTORC2-related signalling pathways and functions are relatively less studied.
752 Therefore, the currently available research has mainly focused on mTORC1[70].
753 mTOR involves multiple pathways, and there are mainly two upstream signalling
754 pathways: the PI3K/Akt/mTOR canonical pathway and the AMPK/TSC1-TSC2/mTOR
755 non-canonical pathway. Regulation of cell growth, proliferation, metabolism and
756 autophagy is achieved through these two pathways[71]. mTOR signalling also plays an
757 important role in the process of cellular senescence. Numerous studies have shown that
758 inhibiting the mTOR signalling pathway by means of dietary restriction, RAPA or gene
759 knockout can significantly delay cellular senescence[72, 73]. Increased mTOR activity
760 is associated with ageing and autophagy deficits with age. The mTOR-specific inhibitor
761 RAPA can delay replicative senescence, reduce senescence caused by DNA damage,
762 and reduce mitochondrial dysfunction[74]. We had previously reported that the mTOR
763 signalling pathway is involved in the process of arterial calcification caused by trans-
764 differentiation of VSMCs into osteoblasts, and inhibiting the mTOR signalling pathway
765 can delay vascular calcification[75]. Consistent with these findings, CT-Exo activated
766 AMPK and inhibited mTOR in VSMCs, while AMPK inhibitors or mTOR activators
767 abolished the CT-Exo-induced ~~protection effects VSMCs against inhibitory effects on~~
768 osteoblastic differentiation/ageing ~~of VSMCs~~. Taken together, these results
769 demonstrate that CT-Exo ~~protects against~~alleviates arterial calcification by activating
770 AMPK/mTOR signalling.

771 In recent years, researchers have found that miRNAs also play an important role in
772 the occurrence and development of vascular ageing and ageing-related diseases[76].
773 Previous studies have found that miR-320a is involved in the negative regulation of
774 osteoblastic differentiation[77] and miRNA profiling revealed that miR-320a is
775 overexpressed in osteoporotic samples[78]. However, the role of miR-320a-3p in the
776 senescence of VSMCs has not yet been reported. We discovered the role of plasma
777 exosome-derived miR-320a-3p in MAC for the first time and successfully identified its
778 relevant downstream target gene, namely PDCD4. In contrast, miR-320a-3p silencing
779 in VSMCs almost completely reversed these anti-calcification effects. Furthermore, we
780 confirmed that miR-320a-3p knockdown in the context of CT-Exo treatment eliminates
781 the anti-MAC effect in mice. PDCD4 is a transcriptional and translational inhibitor and
782 tumour suppressor. Recent studies have shown that PDCD4 may also be involved in
783 some inflammatory diseases[79] and negatively regulate autophagy[56]. Jiang et al.[80]

784 found that PDCD4 deficiency attenuated atherosclerosis (a chronic inflammation of the
785 arterial wall) in hyperlipidaemic mice partly by upregulating the anti-inflammatory
786 cytokine IL-10. Meanwhile, Wang et al.[56] showed that endogenous PDCD4 promotes
787 the formation of macrophage foam cells and the development of atherosclerosis by
788 inhibiting autophagy. PDCD4 downregulation by miR-21 protects cardiomyocytes
789 from ischaemia/reperfusion or ROS-induced injury[81]. Our study shows that
790 endogenous PDCD4 promotes medial calcification/senescence and thus represents a
791 potential therapeutic target for patients with MAC.

792 If the content of this study is transformed into research, it is obvious that it is
793 impractical to collect exosomes from individuals exposed to cold environments and
794 transplant them to other patients. Moreover, nucleic acids themselves are acidic and
795 highly unstable in the blood, making it difficult to penetrate cell membranes. How to
796 deliver drugs into cells from outside the body is a challenge and how to target drugs to
797 diseased tissues to avoid systemic toxicity is also a problem. For these reasons, we
798 suggest overexpressing miRNA-320a-3p in human blood extracellular vesicles before
799 transplantation to exert a protective effect against arterial media calcification.
800 Exosomes, as a naturally domesticated endogenous nanocarrier, can maintain the
801 biological activity of their contents *in vivo* and have the characteristics of low
802 immunogenicity and high safety. In addition, exosomes can circulate to all
803 compartments in the body, which has good application potential in non-liver targeted
804 nucleic acid drug delivery. Engineering transformation can maximise the advantages of
805 extracellular vesicles as nucleic acid drug carriers and may become the mainstream
806 choice for extracellular nucleic acid drug carriers in the future.

807 There are some limitations to this study. In addition to the changes in the composition
808 of plasma-derived exosomes induced by cold, we hypothesised that perivascular
809 adipose tissue and brown adipose tissue in mice also secrete factors or vesicles that play
810 a role in the calcification of the media under cold exposure. This will be our next
811 research direction. The chronic cold stimulation at 4–8°C leads to a state of low
812 metabolism; and the ageing and calcification of VSMCs also slows down. Next, we will
813 continue to study the effects of extremely cold (-10–to-0°C) and warm (34°C)
814 environments on MAC in mice; and the effects of acute, chronic and intermittent cold
815 exposure on MAC. We believe that these results will be helpful to guide future clinical
816 work. Another limitation of our study is that we did not perform a ‘dose-response’
817 experiment to assess the effects of CT-Exo and RT-Exo on the vascular phenotype and
818 the pathology of vascular calcification in normal physiology. Currently, there is no
819 evidence for the physiological concentrations of CT-Exo and RT-Exo in vascular tissue.
820 Future studies should use accurate assays to determine the physiological concentrations
821 of CT-Exo and RT-Exo and to investigate whether there is a dose-dependent response
822 in CT-Exo- and RT-Exo-treated mice. Finally, it remains to be determined whether the
823 beneficial effects of miR-320a-3p observed in cold-exposed mice can be translated to
824 humans. Additional work should determine the frequency, minimum intensity, duration
825 and type of cold exposure required to prevent changes in MAC in patients; and whether
826 there are any contraindications to such interventions in certain populations[82].
827

设置了格式: 字体: 倾斜

872 of ALP staining of VSMCs that had been pre-treated with the indicated concentrations
873 of 3-MA or rapamycin for 30 min and then incubated with β -GP for 14 days (n = 5 per
874 group). The scale bar is 200 μ m. (b) Quantitative analysis of the ALP activity. (c, d)
875 ARS staining showing calcified aorta from CTRL, PS, CT-Exo, 3-MA, CT-Exo+3-MA
876 and RAPA mice (n = 5 per group). The black scale bar is 200 μ m. (e) Vascular calcium
877 content measurement. (f) The expression of p/t-AMPK and p/t-mTOR was determined
878 with western blot in calcified VSMCs treated with CT-Exo, 3-MA or 3-MA+CT-Exo
879 (n = 4 per group). (g) Quantitative analysis of western blotting results. The CTRL group
880 represented the negative control group with only PBS treatment. The PS group
881 represented the positive control group with only β -GP treatment. The data are expressed
882 as the mean \pm standard deviation. The data were analysed with one-way ANOVA with
883 the Bonferroni *post hoc* test or the unpaired, two-tailed Student's t-test. * $p < 0.05$; ** p
884 < 0.01 ; *** $p < 0.001$; **** $p < 0.0001$. **Fig. s8.** The AMPK/mTOR signalling pathway
885 mediated ~~defensive roles~~inhibition effects of CT-Exo on calcification/aging of VSMCs.
886 (a) Expression of p-mTOR and p-AMPK in the β -GP-induced VSMCs treated with
887 Compound C or MHY1485 were analysed by western blot (n = 4 per group). (b) The
888 data are presented as densitometric ratios of RUNX2/GAPDH, p/t-mTOR and p/t-
889 AMPK respectively. (c, d) Representative micrographs of ARS and SA- β -gal staining
890 view were shown (n = 5 per group). (e, f) The data are presented as the ratio of positive
891 staining area, shown as the mean \pm standard deviation. The data were analysed with
892 one-way ANOVA with the Bonferroni *post hoc* test or the unpaired, two-tailed
893 Student's t-test. * $p < 0.05$; ** $p < 0.01$; *** $p < 0.001$; **** $p < 0.0001$. **Fig. s9.** siPDCD4
894 can activate the AMPK/mTOR signalling pathway to promote VSMCs autophagy.
895 Western blot analysis (a) and quantification (b) of LC3B, ATG5, p53, p/t-AMPK and
896 p/t-mTOR in VSMCs treated with siPDCD#3 or siRNA control (n = 4 per group). The
897 CTRL group represented the negative control group with only PBS treatment. The data
898 are presented as the mean \pm standard deviation. The data were analysed one-way
899 ANOVA with the Bonferroni *post hoc* test. * $p < 0.05$; **** $p < 0.0001$.

900

901 **Acknowledgments**

902 We sincerely thank the animal care staff and technicians of the Animal Experimental
903 Center of the Second Xiangya Hospital of Central South University for their care and
904 special treatment of these mice.

905

906 **Author's Contributors**

907 Conceptualization: L-Q.Y., F-X-Z.L. and K-X. T. Supervision: F-X-Z.L., S-K.S., F.X.,
908 M-H.Z., L-M.L. and X.L. Investigation: F-X-Z.L., B.G., C-C.L., K-X.T., Y-C.C., Y-
909 Y.W., J-Y.D., Y-H.W., S-Y.H., X.C. and F.W. Visualization: F-X-Z.L. and L-Q.Y.
910 Resources: F-X-Z.L., J-J.L., F.X. and L-Q.Y. Writing—original draft: F-X-Z.L., J-J.L.
911 and L-Q.Y. Reviewing, editing, and funding acquisition: F.X. and L-Q.Y. All authors
912 read and approved the final manuscript.

913

914 **Funding**

915 This study was supported by the National Natural Science Foundation of China (No.
916 82071593, 81974223, 81770833 and 82100944), Key R&D Plan Hunan Province
917 (2020SK2078) and Natural Science Foundation of Hunan Province (No. 2021JJ30036
918 and 2021JJ40842).

919

920 **Availability of data and materials**

921 All data generated and analyzed during this research are included in this published
922 article.

923

924 **Declarations**

925

926 **Ethics approval and consent to participate**

927 All experiments were reviewed and approved by the Ethics Committee of the Second
928 Xiang-Yya Hospital, Central South University. All the procedures conformed to the
929 Guide for the Care and Use of Laboratory Animals, NIH publication (8th edition, 2011).

930 All the animal protocols were formally approved by the Ethics Committee of the
931 Second Xiang-Yya Hospital, Central South University (2022708).

932

933 **Consent for publication**

934 All authors agree for publication.

935

936 **Competing interests**

937 The authors declare no conflict of interest.

938

939 **Author details**

940 ¹Department of Metabolism and Endocrinology, National Clinical Research Center for
941 Metabolic Disease, Hunan Provincial Key Laboratory of Metabolic Bone Diseases, The
942 Second Xiang-Yya Hospital, Central South University, Changsha, China. ²Department
943 of Periodontal Division, Hunan Xiangya Stomatological Hospital, Central South
944 University, Changsha, China. ³Department of Radiology, The Second Xiang-Yya
945 Hospital, Central South University, Changsha, China. ⁴[Department of Pathology, The
946 Second Xiangya Hospital, Central South University, Changsha, China.](#)

947

948

949 **References**

- 950 1. Wee NKY, Nguyen AD, Enriquez RF, Zhang L, Herzog H, Baldock PA. Neuropeptide Y
951 Regulation of Energy Partitioning and Bone Mass During Cold Exposure. *Calcif Tissue Int.*
952 2020;107(5):510-23.
- 953 2. Dong M, Yang X, Lim S, Cao Z, Honek J, Lu H, Zhang C, Seki T, Hosaka K, Wahlberg E,
954 Yang J, Zhang L, Länne T, Sun B, Li X, Liu Y, Zhang Y, Cao Y. Cold exposure promotes
955 atherosclerotic plaque growth and instability via UCP1-dependent lipolysis. *Cell Metab.*
956 2013;18(1):118-29.
- 957 3. Sacks D, Baxter B, Campbell BCV, Carpenter JS, Cognard C, Dippel D, Eesa M, Fischer U,
958 Hausegger K, Hirsch JA, Shazam Hussain M, Jansen O, Jayaraman MV, Khalessi AA, Kluck

- 959 BW, Lavine S, Meyers PM, Ramee S, Rüfenacht DA, Schirmer CM, Vorwerk D. Multisociety
960 Consensus Quality Improvement Revised Consensus Statement for Endovascular Therapy
961 of Acute Ischemic Stroke. *Int J Stroke*. 2018;13(6):612-32.
- 962 4. Du J, He Z, Xu M, Qu X, Cui J, Zhang S, Zhang S, Li H, Yu Z. Brown Adipose Tissue Rescues
963 Bone Loss Induced by Cold Exposure. *Front Endocrinol (Lausanne)*. 2021;12:778019.
- 964 5. Serrat MA. Environmental temperature impact on bone and cartilage growth. *Compr
965 Physiol*. 2014;4(2):621-55.
- 966 6. Salehipour-Shirazi G, Ferguson LV, Sinclair BJ. Does cold activate the *Drosophila*
967 *melanogaster* immune system? *J Insect Physiol*. 2017;96:29-34.
- 968 7. Ivanova YM, Blondin DP. Examining the benefits of cold exposure as a therapeutic strategy
969 for obesity and type 2 diabetes. *J Appl Physiol (1985)*. 2021;130(5):1448-59.
- 970 8. Liu C, Yavar Z, Sun Q. Cardiovascular response to thermoregulatory challenges. *Am J
971 Physiol Heart Circ Physiol*. 2015;309(11):H1793-812.
- 972 9. Ungvari Z, Kaley G, de Cabo R, Sonntag WE, Csiszar A. Mechanisms of vascular aging: new
973 perspectives. *J Gerontol A Biol Sci Med Sci*. 2010;65(10):1028-41.
- 974 10. Reesink KD, Spronck B. Constitutive interpretation of arterial stiffness in clinical studies: a
975 methodological review. *Am J Physiol Heart Circ Physiol*. 2019;316(3):H693-h709.
- 976 11. Cao YC, Shan SK, Guo B, Li CC, Li FX, Zheng MH, Xu QS, Wang Y, Lei LM, Tang KX, Ou-
977 Yang WL, Duan JY, Wu YY, Ullah MHE, Zhou ZA, Xu F, Lin X, Wu F, Liao XB, Yuan LQ.
978 Histone Lysine Methylation Modification and Its Role in Vascular Calcification. *Front
979 Endocrinol (Lausanne)*. 2022;13:863708.
- 980 12. Weber T, Chirinos JA. Pulsatile arterial haemodynamics in heart failure. *Eur Heart J*.
981 2018;39(43):3847-54.
- 982 13. Chirinos JA, Segers P, Hughes T, Townsend R. Large-Artery Stiffness in Health and Disease:
983 JACC State-of-the-Art Review. *J Am Coll Cardiol*. 2019;74(9):1237-63.
- 984 14. Lanzer P, Hannan FM, Lanzer JD, Janzen J, Raggi P, Furniss D, Schuchardt M, Thakker R,
985 Fok PW, Saez-Rodriguez J, Millan A, Sato Y, Ferraresi R, Virmani R, St Hilaire C. Medial
986 Arterial Calcification: JACC State-of-the-Art Review. *J Am Coll Cardiol*. 2021;78(11):1145-
987 65.
- 988 15. Boström K, Watson KE, Horn S, Wortham C, Herman IM, Demer LL. Bone morphogenetic
989 protein expression in human atherosclerotic lesions. *J Clin Invest*. 1993;91(4):1800-9.
- 990 16. Xu F, Li FX, Lin X, Zhong JY, Wu F, Shan SK, Tan CM, Yuan LQ, Liao XB. Adipose tissue-
991 derived omentin-1 attenuates arterial calcification via AMPK/Akt signaling pathway. *Aging
992 (Albany NY)*. 2019;11(20):8760-76.
- 993 17. Ye Y, Chen A, Li L, Liang Q, Wang S, Dong Q, Fu M, Lan Z, Li Y, Liu X, Ou JS, Lu L, Yan J.
994 Repression of the antiporter SLC7A11/glutathione/glutathione peroxidase 4 axis drives
995 ferroptosis of vascular smooth muscle cells to facilitate vascular calcification. *Kidney Int*.
996 2022;102(6):1259-75.
- 997 18. Lan Z, Chen A, Li L, Ye Y, Liang Q, Dong Q, Wang S, Fu M, Li Y, Liu X, Zhu Z, Ou JS, Qiu X,
998 Lu L, Yan J. Downregulation of HDAC9 by the ketone metabolite β -hydroxybutyrate
999 suppresses vascular calcification. *J Pathol*. 2022;258(3):213-26.
- 1000 19. Liu X, Chen A, Liang Q, Yang X, Dong Q, Fu M, Wang S, Li Y, Ye Y, Lan Z, Chen Y, Ou JS,
1001 Yang P, Lu L, Yan J. Spermidine inhibits vascular calcification in chronic kidney disease
1002 through modulation of SIRT1 signaling pathway. *Aging Cell*. 2021;20(6):e13377.

1003 20. Théry C, Witwer KW, Aikawa E, Alcaraz MJ, Anderson JD, Andriantsitohaina R, Antoniou A,
1004 Arab T, Archer F, Atkin-Smith GK, Ayre DC, Bach JM, Bachurski D, Baharvand H, Balaj L,
1005 Baldacchino S, Bauer NN, Baxter AA, Bebawy M, Beckham C, Bedina Zavec A, Benmoussa
1006 A, Berardi AC, Bergese P, Bielska E, Blenkiron C, Bobis-Wozowicz S, Boilard E, Boireau W,
1007 Bongiovanni A, Borràs FE, Bosch S, Boulanger CM, Breakefield X, Breglio AM, Brennan M,
1008 Brigstock DR, Brisson A, Broekman ML, Bromberg JF, Bryl-Górecka P, Buch S, Buck AH,
1009 Burger D, Busatto S, Buschmann D, Bussolati B, Buzás EI, Byrd JB, Camussi G, Carter DR,
1010 Caruso S, Chamley LW, Chang YT, Chen C, Chen S, Cheng L, Chin AR, Clayton A, Clerici
1011 SP, Cocks A, Cocucci E, Coffey RJ, Cordeiro-da-Silva A, Couch Y, Coumans FA, Coyle B,
1012 Crescitelli R, Criado MF, D'Souza-Schorey C, Das S, Datta Chaudhuri A, de Candia P, De
1013 Santana EF, De Wever O, Del Portillo HA, Demaret T, Deville S, Devitt A, Dhondt B, Di Vizio
1014 D, Dieterich LC, Dolo V, Dominguez Rubio AP, Dominici M, Dourado MR, Driedonks TA,
1015 Duarte FV, Duncan HM, Eichenberger RM, Ekström K, El Andaloussi S, Elie-Caille C,
1016 Erdbrügger U, Falcón-Pérez JM, Fatima F, Fish JE, Flores-Bellver M, Försonits A, Frelet-
1017 Barrand A, Fricke F, Fuhrmann G, Gabriellsson S, Gámez-Valero A, Gardiner C, Gärtner K,
1018 Gaudin R, Gho YS, Giebel B, Gilbert C, Gimona M, Giusti I, Goberdhan DC, Görgens A,
1019 Gorski SM, Greening DW, Gross JC, Gualerzi A, Gupta GN, Gustafson D, Handberg A,
1020 Haraszti RA, Harrison P, Hegyesi H, Hendrix A, Hill AF, Hochberg FH, Hoffmann KF, Holder
1021 B, Holthofer H, Hosseinkhani B, Hu G, Huang Y, Huber V, Hunt S, Ibrahim AG, Ikezu T, Inal
1022 JM, Isin M, Ivanova A, Jackson HK, Jacobsen S, Jay SM, Jayachandran M, Jenster G, Jiang
1023 L, Johnson SM, Jones JC, Jong A, Jovanovic-Talisman T, Jung S, Kalluri R, Kano SI, Kaur S,
1024 Kawamura Y, Keller ET, Khamari D, Khomyakova E, Khvorova A, Kierulf P, Kim KP, Kislinger
1025 T, Klingeborn M, Klinke DJ, 2nd, Kornek M, Kosanović MM, Kovács Á F, Krämer-Albers EM,
1026 Krasemann S, Krause M, Kurochkin IV, Kusuma GD, Kuypers S, Laitinen S, Langevin SM,
1027 Languino LR, Lannigan J, Lässer C, Laurent LC, Lavieu G, Lázaro-Ibáñez E, Le Lay S, Lee
1028 MS, Lee YXF, Lemos DS, Lenassi M, Leszczynska A, Li IT, Liao K, Libregts SF, Ligeti E, Lim
1029 R, Lim SK, Linē A, Linnemannstōns K, Llorente A, Lombard CA, Lorenowicz MJ, Lörincz Á
1030 M, Lötvall J, Lovett J, Lowry MC, Loyer X, Lu Q, Lukomska B, Lunavat TR, Maas SL, Malhi
1031 H, Marcilla A, Mariani J, Mariscal J, Martens-Uzunova ES, Martin-Jaular L, Martinez MC,
1032 Martins VR, Mathieu M, Mathivanan S, Maugeri M, McGinnis LK, McVey MJ, Meckes DG,
1033 Jr., Meehan KL, Mertens I, Minciacci VR, Möller A, Møller Jørgensen M, Morales-
1034 Kastresana A, Morhayim J, Mullier F, Muraca M, Musante L, Mussack V, Muth DC, Myburgh
1035 KH, Najrana T, Nawaz M, Nazarenko I, Nejsun P, Neri C, Neri T, Nieuwland R, Nimrichter
1036 L, Nolan JP, Nolte-'t Hoen EN, Noren Hooten N, O'Driscoll L, O'Grady T, O'Loughlen A,
1037 Ochiya T, Olivier M, Ortiz A, Ortiz LA, Osteikoetxea X, Østergaard O, Ostrowski M, Park J,
1038 Pegtel DM, Peinado H, Perut F, Pfaffl MW, Phinney DG, Pieters BC, Pink RC, Pisetsky DS,
1039 Pogge von Strandmann E, Polakovicova I, Poon IK, Powell BH, Prada I, Pulliam L,
1040 Quesenberry P, Radeghieri A, Raffai RL, Raimondo S, Rak J, Ramirez MI, Raposo G, Rayyan
1041 MS, Regev-Rudzki N, Ricklefs FL, Robbins PD, Roberts DD, Rodrigues SC, Rohde E, Rome
1042 S, Rouschop KM, Rughetti A, Russell AE, Saá P, Sahoo S, Salas-Huenuleo E, Sánchez C,
1043 Saugstad JA, Saul MJ, Schiffelers RM, Schneider R, Schøyen TH, Scott A, Shahaj E, Sharma
1044 S, Shatnyeva O, Shekari F, Shelke GV, Shetty AK, Shiba K, Siljander PR, Silva AM, Skowronek
1045 A, Snyder OL, 2nd, Soares RP, Sódar BW, Soekmadji C, Sotillo J, Stahl PD, Stoorvogel W,
1046 Stott SL, Strasser EF, Swift S, Tahara H, Tewari M, Timms K, Tiwari S, Tixeira R, Tkach M,

- 1047 Toh WS, Tomasini R, Torrecilhas AC, Tosar JP, Toxavidis V, Urbanelli L, Vader P, van Balkom
1048 BW, van der Grein SG, Van Deun J, van Herwijnen MJ, Van Keuren-Jensen K, van Niel G,
1049 van Royen ME, van Wijnen AJ, Vasconcelos MH, Vechetti IJ, Jr., Veit TD, Vella LJ, Velot É,
1050 Verweij FJ, Vestad B, Viñas JL, Visnovitz T, Vukman KV, Wahlgren J, Watson DC, Wauben
1051 MH, Weaver A, Webber JP, Weber V, Wehman AM, Weiss DJ, Welsh JA, Wendt S,
1052 Wheelock AM, Wiener Z, Witte L, Wolfram J, Xagorari A, Xander P, Xu J, Yan X, Yáñez-Mó
1053 M, Yin H, Yuana Y, Zappulli V, Zarubova J, Žėkas V, Zhang JY, Zhao Z, Zheng L, Zheutlin
1054 AR, Zickler AM, Zimmermann P, Zivkovic AM, Zocco D, Zuba-Surma EK. Minimal
1055 information for studies of extracellular vesicles 2018 (MISEV2018): a position statement of
1056 the International Society for Extracellular Vesicles and update of the MISEV2014 guidelines.
1057 *J Extracell Vesicles*. 2018;7(1):1535750.
- 1058 21. Luo ZW, Li FX, Liu YW, Rao SS, Yin H, Huang J, Chen CY, Hu Y, Zhang Y, Tan YJ, Yuan LQ,
1059 Chen TH, Liu HM, Cao J, Liu ZZ, Wang ZX, Xie H. Aptamer-functionalized exosomes from
1060 bone marrow stromal cells target bone to promote bone regeneration. *Nanoscale*.
1061 2019;11(43):20884-92.
- 1062 22. Liu J, Li F, Liu B, Yao Z, Li L, Liu G, Peng L, Wang Y, Huang J. Adipose -derived mesenchymal
1063 stem cell exosomes inhibit transforming growth factor- β 1-induced collagen synthesis in
1064 oral mucosal fibroblasts. *Exp Ther Med*. 2021;22(6):1419.
- 1065 23. Li FX, Lin X, Xu F, Shan SK, Guo B, Lei LM, Zheng MH, Wang Y, Xu QS, Yuan LQ. The Role
1066 of Mesenchymal Stromal Cells-Derived Small Extracellular Vesicles in Diabetes and Its
1067 Chronic Complications. *Front Endocrinol (Lausanne)*. 2021;12:780974.
- 1068 24. Li FX, Liu JJ, Xu F, Lin X, Zhong JY, Wu F, Yuan LQ. Role of tumor-derived exosomes in
1069 bone metastasis. *Oncol Lett*. 2019;18(4):3935-45.
- 1070 25. Wu YL, Lin ZJ, Li CC, Lin X, Shan SK, Guo B, Zheng MH, Li F, Yuan LQ, Li ZH. Epigenetic
1071 regulation in metabolic diseases: mechanisms and advances in clinical study. *Signal*
1072 *Transduct Target Ther*. 2023;8(1):98.
- 1073 26. Wang ZX, Luo ZW, Li FX, Cao J, Rao SS, Liu YW, Wang YY, Zhu GQ, Gong JS, Zou JT, Wang
1074 Q, Tan YJ, Zhang Y, Hu Y, Li YY, Yin H, Wang XK, He ZH, Ren L, Liu ZZ, Hu XK, Yuan LQ,
1075 Xu R, Chen CY, Xie H. Aged bone matrix-derived extracellular vesicles as a messenger for
1076 calcification paradox. *Nat Commun*. 2022;13(1):1453.
- 1077 27. Lin X, Shan SK, Xu F, Zhong JY, Wu F, Duan JY, Guo B, Li FX, Wang Y, Zheng MH, Xu QS,
1078 Lei LM, Ou-Yang WL, Wu YY, Tang KX, Ullah MHE, Liao XB, Yuan LQ. The crosstalk
1079 between endothelial cells and vascular smooth muscle cells aggravates high phosphorus-
1080 induced arterial calcification. *Cell Death Dis*. 2022;13(7):650.
- 1081 28. Guo B, Shan SK, Xu F, Lin X, Li FX, Wang Y, Xu QS, Zheng MH, Lei LM, Li CC, Zhou ZA,
1082 Ullah MHE, Wu F, Liao XB, Yuan LQ. Protective role of small extracellular vesicles derived
1083 from HUVECs treated with AGEs in diabetic vascular calcification. *J Nanobiotechnology*.
1084 2022;20(1):334.
- 1085 29. Wu YY, Shan SK, Lin X, Xu F, Zhong JY, Wu F, Duan JY, Guo B, Li FX, Wang Y, Zheng MH,
1086 Xu QS, Lei LM, Ou-Yang WL, Tang KX, Li CC, Ullah MHE, Yuan LQ. Cellular Crosstalk in the
1087 Vascular Wall Microenvironment: The Role of Exosomes in Vascular Calcification. *Front*
1088 *Cardiovasc Med*. 2022;9:912358.
- 1089 30. Fleming A, Bourdenx M, Fujimaki M, Karabiyik C, Krause GJ, Lopez A, Martín-Segura A,
1090 Puri C, Scrivo A, Skidmore J, Son SM, Stamatakou E, Wrobel L, Zhu Y, Cuervo AM,

- 1091 Rubinsztein DC. The different autophagy degradation pathways and neurodegeneration.
1092 *Neuron*. 2022;110(6):935-66.
- 1093 31. Menzies FM, Fleming A, Caricasole A, Bento CF, Andrews SP, Ashkenazi A, Füllgrabe J,
1094 Jackson A, Jimenez Sanchez M, Karabiyik C, Licitra F, Lopez Ramirez A, Pavel M, Puri C,
1095 Renna M, Ricketts T, Schlotawa L, Vicinanza M, Won H, Zhu Y, Skidmore J, Rubinsztein DC.
1096 Autophagy and Neurodegeneration: Pathogenic Mechanisms and Therapeutic
1097 Opportunities. *Neuron*. 2017;93(5):1015-34.
- 1098 32. White E, Lattime EC, Guo JY. Autophagy Regulates Stress Responses, Metabolism, and
1099 Anticancer Immunity. *Trends Cancer*. 2021;7(8):778-89.
- 1100 33. Deretic V. Autophagy in inflammation, infection, and immunometabolism. *Immunity*.
1101 2021;54(3):437-53.
- 1102 34. Gao W, Wang X, Zhou Y, Wang X, Yu Y. Autophagy, ferroptosis, pyroptosis, and
1103 necroptosis in tumor immunotherapy. *Signal Transduct Target Ther*. 2022;7(1):196.
- 1104 35. Kaushik S, Tasset I, Arias E, Pampliega O, Wong E, Martinez-Vicente M, Cuervo AM.
1105 Autophagy and the hallmarks of aging. *Ageing Res Rev*. 2021;72:101468.
- 1106 36. Wilhelm T, Richly H. Autophagy during ageing - from Dr Jekyll to Mr Hyde. *Febs j*.
1107 2018;285(13):2367-76.
- 1108 37. Qiao L, Ma J, Zhang Z, Sui W, Zhai C, Xu D, Wang Z, Lu H, Zhang M, Zhang C, Chen W,
1109 Zhang Y. Deficient Chaperone-Mediated Autophagy Promotes Inflammation and
1110 Atherosclerosis. *Circ Res*. 2021;129(12):1141-57.
- 1111 38. Tao H, Yancey PG, Blakemore JL, Zhang Y, Ding L, Jerome WG, Brown JD, Vickers KC,
1112 Linton MF. Macrophage SR-BI modulates autophagy via VPS34 complex and PPAR α
1113 transcription of Tfeb in atherosclerosis. *J Clin Invest*. 2021;131(7).
- 1114 39. Chen Z, Ouyang C, Zhang H, Gu Y, Deng Y, Du C, Cui C, Li S, Wang W, Kong W, Chen J,
1115 Cai J, Geng B. Vascular smooth muscle cell-derived hydrogen sulfide promotes
1116 atherosclerotic plaque stability via TFEB (transcription factor EB)-mediated autophagy.
1117 *Autophagy*. 2022;1-18.
- 1118 40. Forte M, Bianchi F, Cotugno M, Marchitti S, De Falco E, Raffa S, Stanzione R, Di Nonno F,
1119 Chimenti I, Palmerio S, Pagano F, Petrozza V, Micaloni A, Madonna M, Relucanti M, Torrisi
1120 MR, Frati G, Volpe M, Rubattu S, Sciarretta S. Pharmacological restoration of autophagy
1121 reduces hypertension-related stroke occurrence. *Autophagy*. 2020;16(8):1468-81.
- 1122 41. Li FF, Shang XK, Du XL, Chen S. Rapamycin Treatment Attenuates Angiotensin II -induced
1123 Abdominal Aortic Aneurysm Formation via VSMC Phenotypic Modulation and Down-
1124 regulation of ERK1/2 Activity. *Curr Med Sci*. 2018;38(1):93-100.
- 1125 42. Peng YQ, Xiong D, Lin X, Cui RR, Xu F, Zhong JY, Zhu T, Wu F, Mao MZ, Liao XB, Yuan LQ.
1126 Oestrogen Inhibits Arterial Calcification by Promoting Autophagy. *Sci Rep*. 2017;7(1):3549.
- 1127 43. Horowitz AM, Fan X, Bieri G, Smith LK, Sanchez-Diaz CI, Schroer AB, Gontier G, Casaletto
1128 KB, Kramer JH, Williams KE, Villeda SA. Blood factors transfer beneficial effects of exercise
1129 on neurogenesis and cognition to the aged brain. *Science*. 2020;369(6500):167-73.
- 1130 44. Dinkins MB, Dasgupta S, Wang G, Zhu G, Bieberich E. Exosome reduction in vivo is
1131 associated with lower amyloid plaque load in the 5XFAD mouse model of Alzheimer's
1132 disease. *Neurobiol Aging*. 2014;35(8):1792-800.
- 1133 45. Xu F, Zhong JY, Lin X, Shan SK, Guo B, Zheng MH, Wang Y, Li F, Cui RR, Wu F, Zhou E,
1134 Liao XB, Liu YS, Yuan LQ. Melatonin alleviates vascular calcification and ageing through

- 1135 exosomal miR-204/miR-211 cluster in a paracrine manner. *J Pineal Res.*
1136 2020;68(3):e12631.
- 1137 46. Wu F, Lin X, Shan SK, Li F, Xu F, Zhong JY, Guo B, Zheng MH, Wang Y, Mo ZH, Yuan LQ.
1138 The Suppression of miR-199a-3p by Promoter Methylation Contributes to Papillary
1139 Thyroid Carcinoma Aggressiveness by Targeting RAP2a and DNMT3a. *Front Cell Dev Biol.*
1140 2020;8:594528.
- 1141 47. Viegas CSB, Santos L, Macedo AL, Matos AA, Silva AP, Neves PL, Staes A, Gevaert K, Morais
1142 R, Vermeer C, Schurgers L, Simes DC. Chronic Kidney Disease Circulating Calciprotein
1143 Particles and Extracellular Vesicles Promote Vascular Calcification: A Role for GRP (Gla-
1144 Rich Protein). *Arterioscler Thromb Vasc Biol.* 2018;38(3):575-87.
- 1145 48. Tai S, Hu XQ, Peng DQ, Zhou SH, Zheng XL. The roles of autophagy in vascular smooth
1146 muscle cells. *Int J Cardiol.* 2016;211:1-6.
- 1147 49. Piwkowska A, Rogacka D, Jankowski M, Dominiczak MH, Stepiński JK, Angielski S.
1148 Metformin induces suppression of NAD(P)H oxidase activity in podocytes. *Biochem*
1149 *Biophys Res Commun.* 2010;393(2):268-73.
- 1150 50. Kim J, Kundu M, Viollet B, Guan KL. AMPK and mTOR regulate autophagy through direct
1151 phosphorylation of Ulk1. *Nat Cell Biol.* 2011;13(2):132-41.
- 1152 51. Egan D, Kim J, Shaw RJ, Guan KL. The autophagy initiating kinase ULK1 is regulated via
1153 opposing phosphorylation by AMPK and mTOR. *Autophagy.* 2011;7(6):643-4.
- 1154 52. Wang S, Song P, Zou MH. AMP-activated protein kinase, stress responses and
1155 cardiovascular diseases. *Clin Sci (Lond).* 2012;122(12):555-73.
- 1156 53. Zhang C, Wang X. miR-320a Targeting RGS5 Aggravates Atherosclerosis by Promoting
1157 Migration and Proliferation of ox-LDL-Stimulated Vascular Smooth Muscle Cells. *J*
1158 *Cardiovasc Pharmacol.* 2022;80(1):110-17.
- 1159 54. Lankat-Buttgereit B, Göke R. The tumour suppressor Pcd4: recent advances in the
1160 elucidation of function and regulation. *Biol Cell.* 2009;101(6):309-17.
- 1161 55. Song X, Zhang X, Wang X, Zhu F, Guo C, Wang Q, Shi Y, Wang J, Chen Y, Zhang L. Tumor
1162 suppressor gene PDCD4 negatively regulates autophagy by inhibiting the expression of
1163 autophagy-related gene ATG5. *Autophagy.* 2013;9(5):743-55.
- 1164 56. Wang L, Jiang Y, Song X, Guo C, Zhu F, Wang X, Wang Q, Shi Y, Wang J, Gao F, Zhao W,
1165 Chen YH, Zhang L. Pcd4 deficiency enhances macrophage lipophagy and attenuates
1166 foam cell formation and atherosclerosis in mice. *Cell Death Dis.* 2016;7(1):e2055.
- 1167 57. Bell JF, Moore GJ. Effects of high ambient temperature on various stages of rabies virus
1168 infection in mice. *Infect Immun.* 1974;10(3):510-5.
- 1169 58. Amrein YU. Effects of environmental temperature on *Trypanosoma cruzi* infection in mice.
1170 *J Parasitol.* 1967;53(6):1160.
- 1171 59. Kokolus KM, Capitano ML, Lee CT, Eng JW, Waight JD, Hylander BL, Sexton S, Hong CC,
1172 Gordon CJ, Abrams SI, Repasky EA. Baseline tumor growth and immune control in
1173 laboratory mice are significantly influenced by subthermoneutral housing temperature.
1174 *Proc Natl Acad Sci U S A.* 2013;110(50):20176-81.
- 1175 60. Simonsick EM, Meier HCS, Shaffer NC, Studenski SA, Ferrucci L. Basal body temperature
1176 as a biomarker of healthy aging. *Age (Dordr).* 2016;38(5-6):445-54.
- 1177 61. Chang L, Villacorta L, Li R, Hamblin M, Xu W, Dou C, Zhang J, Wu J, Zeng R, Chen YE. Loss
1178 of perivascular adipose tissue on peroxisome proliferator-activated receptor- γ deletion

- 1179 in smooth muscle cells impairs intravascular thermoregulation and enhances
1180 atherosclerosis. *Circulation*. 2012;126(9):1067-78.
- 1181 62. Reynés B, van Schothorst EM, García-Ruiz E, Keijzer J, Palou A, Oliver P. Cold exposure
1182 down-regulates immune response pathways in ferret aortic perivascular adipose tissue.
1183 *Thromb Haemost*. 2017;117(5):981-91.
- 1184 63. Tian XY, Ganeshan K, Hong C, Nguyen KD, Qiu Y, Kim J, Tangirala RK, Tontonoz P, Chawla
1185 A. Thermoneutral Housing Accelerates Metabolic Inflammation to Potentiate
1186 Atherosclerosis but Not Insulin Resistance. *Cell Metab*. 2016;23(1):165-78.
- 1187 64. Zhang X, Zhang Y, Wang P, Zhang SY, Dong Y, Zeng G, Yan Y, Sun L, Wu Q, Liu H, Liu B,
1188 Kong W, Wang X, Jiang C. Adipocyte Hypoxia-Inducible Factor 2 α Suppresses
1189 Atherosclerosis by Promoting Adipose Ceramide Catabolism. *Cell Metab*. 2019;30(5):937-
1190 51.e5.
- 1191 65. Chen R, Yin P, Wang L, Liu C, Niu Y, Wang W, Jiang Y, Liu Y, Liu J, Qi J, You J, Kan H, Zhou
1192 M. Association between ambient temperature and mortality risk and burden: time series
1193 study in 272 main Chinese cities. *Bmj*. 2018;363:k4306.
- 1194 66. Chevalier C, Stojanović O, Colin DJ, Suarez-Zamorano N, Tarallo V, Veyrat-Durebex C,
1195 Rigo D, Fabbiano S, Stevanović A, Hagemann S, Montet X, Seimbille Y, Zamboni N,
1196 Hapfelmeier S, Trajkovski M. Gut Microbiota Orchestrates Energy Homeostasis during
1197 Cold. *Cell*. 2015;163(6):1360-74.
- 1198 67. Bukowiecki LJ. Energy balance and diabetes. The effects of cold exposure, exercise training,
1199 and diet composition on glucose tolerance and glucose metabolism in rat peripheral
1200 tissues. *Can J Physiol Pharmacol*. 1989;67(4):382-93.
- 1201 68. Shanahan CM. Mechanisms of vascular calcification in CKD-evidence for premature
1202 ageing? *Nat Rev Nephrol*. 2013;9(11):661-70.
- 1203 69. Dai XY, Zhao MM, Cai Y, Guan QC, Zhao Y, Guan Y, Kong W, Zhu WG, Xu MJ, Wang X.
1204 Phosphate-induced autophagy counteracts vascular calcification by reducing matrix
1205 vesicle release. *Kidney Int*. 2013;83(6):1042-51.
- 1206 70. Lin X, Xu F, Cui RR, Xiong D, Zhong JY, Zhu T, Li F, Wu F, Xie XB, Mao MZ, Liao XB, Yuan
1207 LQ. Arterial Calcification Is Regulated Via an miR-204/DNMT3a Regulatory Circuit Both In
1208 Vitro and in Female Mice. *Endocrinology*. 2018;159(8):2905-16.
- 1209 71. Cui RR, Li SJ, Liu LJ, Yi L, Liang QH, Zhu X, Liu GY, Liu Y, Wu SS, Liao XB, Yuan LQ, Mao DA,
1210 Liao EY. MicroRNA-204 regulates vascular smooth muscle cell calcification in vitro and in
1211 vivo. *Cardiovasc Res*. 2012;96(2):320-9.
- 1212 72. Hao J, Zhang L, Cong G, Ren L, Hao L. MicroRNA-34b/c inhibits aldosterone-induced
1213 vascular smooth muscle cell calcification via a SATB2/Runx2 pathway. *Cell Tissue Res*.
1214 2016;366(3):733-46.
- 1215 73. Pantsulaia I, Ciszewski WM, Niewiarowska J. Senescent endothelial cells: Potential
1216 modulators of immunosenescence and ageing. *Ageing Res Rev*. 2016;29:13-25.
- 1217 74. Yang L, Cheng P, Chen C, He HB, Xie GQ, Zhou HD, Xie H, Wu XP, Luo XH. miR-93/Sp7
1218 function loop mediates osteoblast mineralization. *J Bone Miner Res*. 2012;27(7):1598-606.
- 1219 75. Maegdefessel L, Rayner KJ, Leeper NJ. MicroRNA regulation of vascular smooth muscle
1220 function and phenotype: early career committee contribution. *Arterioscler Thromb Vasc*
1221 *Biol*. 2015;35(1):2-6.
- 1222 76. Lee S, Choi E, Cha MJ, Park AJ, Yoon C, Hwang KC. Impact of miRNAs on cardiovascular

1223 aging. *J Geriatr Cardiol.* 2015;12(5):569-74.

1224 77. Wang CG, Hu YH, Su SL, Zhong D. LncRNA DANCR and miR-320a suppressed osteogenic
1225 differentiation in osteoporosis by directly inhibiting the Wnt/ β -catenin signaling pathway.
1226 *Exp Mol Med.* 2020;52(8):1310-25.

1227 78. De-Ugarte L, Yoskovitz G, Balcells S, Güerri-Fernández R, Martínez-Díaz S, Mellibovsky L,
1228 Urreizti R, Nogués X, Grinberg D, García-Giralt N, Díez-Pérez A. MiRNA profiling of whole
1229 trabecular bone: identification of osteoporosis-related changes in MiRNAs in human hip
1230 bones. *BMC Med Genomics.* 2015;8:75.

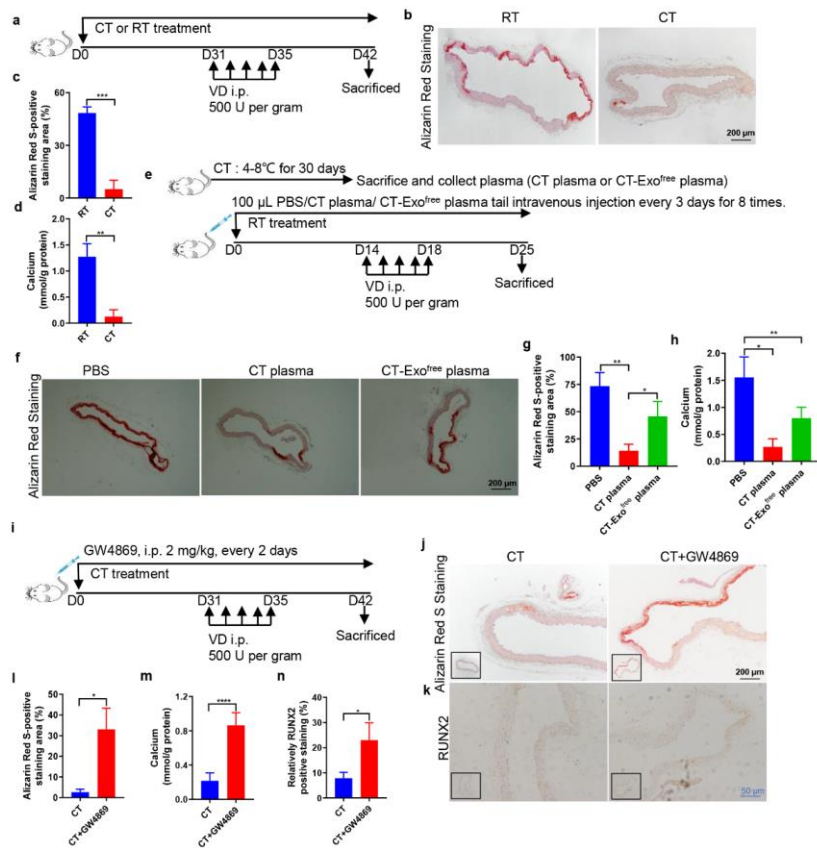
1231 79. Sheedy FJ, Palsson-McDermott E, Hennessy EJ, Martin C, O'Leary JJ, Ruan Q, Johnson DS,
1232 Chen Y, O'Neill LA. Negative regulation of TLR4 via targeting of the proinflammatory
1233 tumor suppressor PDCD4 by the microRNA miR-21. *Nat Immunol.* 2010;11(2):141-7.

1234 80. Jiang Y, Gao Q, Wang L, Guo C, Zhu F, Wang B, Wang Q, Gao F, Chen Y, Zhang L.
1235 Deficiency of programmed cell death 4 results in increased IL-10 expression by
1236 macrophages and thereby attenuates atherosclerosis in hyperlipidemic mice. *Cell Mol*
1237 *Immunol.* 2016;13(4):524-34.

1238 81. Cheng Y, Zhu P, Yang J, Liu X, Dong S, Wang X, Chun B, Zhuang J, Zhang C. Ischaemic
1239 preconditioning-regulated miR-21 protects heart against ischaemia/reperfusion injury via
1240 anti-apoptosis through its target PDCD4. *Cardiovasc Res.* 2010;87(3):431-9.

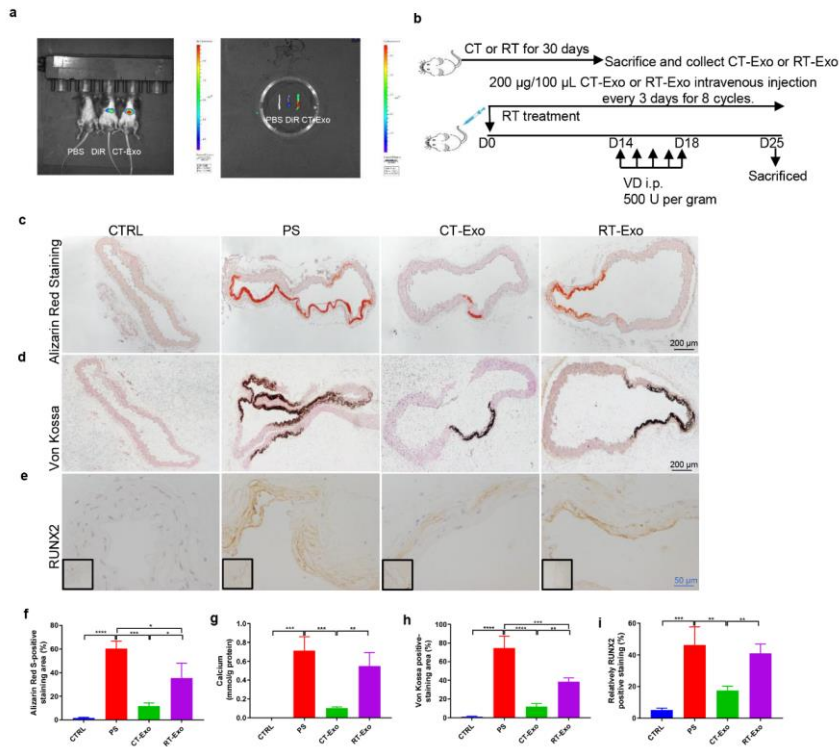
1241 82. Blondin DP, Haman F. Shivering and nonshivering thermogenesis in skeletal muscles.
1242 *Handb Clin Neurol.* 2018;156:153-73.

1243



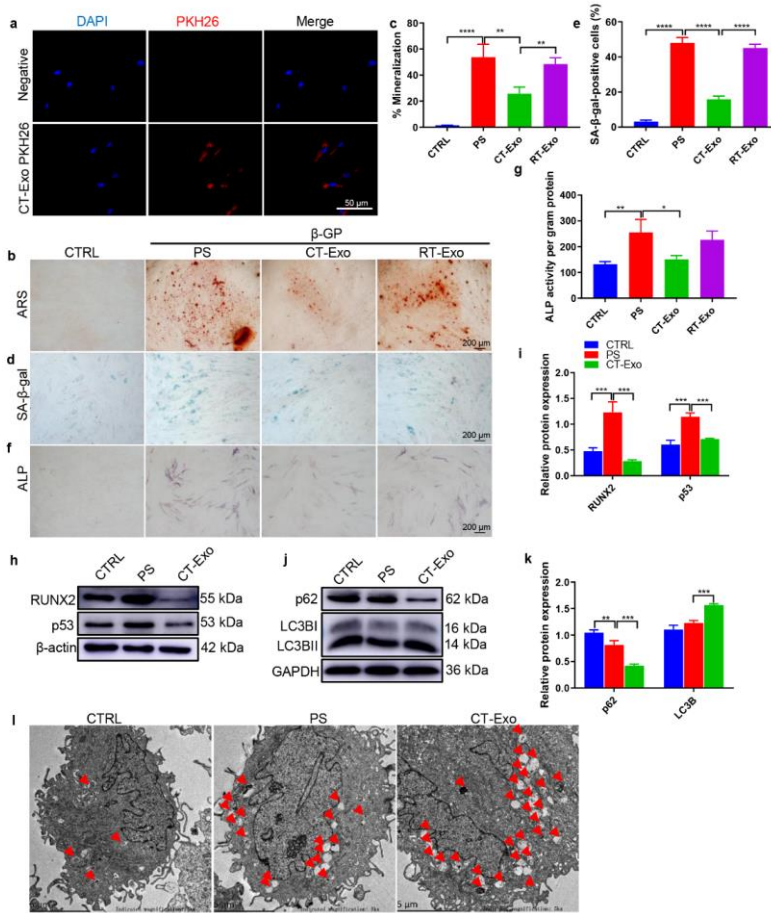
1244
 1245 **Fig. 1 Cold exposure protected against alleviated MAC in a VD-induced mouse**
 1246 **model.** (a) The schematic flow diagram represents the *in vivo* treatment of CT or RT in the VD-treated mouse model (n = 6 per group). ARS-stained sections from thoracic
 1247 aorta (b) and quantitation of positive staining area (c) are shown. The black scale bar is
 1248 200 μ m. (d) Vascular calcium content measurement. (e) Experimental design of the
 1249 VD-induced vascular calcification mouse model treated with PBS, CT plasma or CT-
 1250 Exo^{free} plasma by intravenous injection (n = 6 per group). ARS-stained sections from
 1251 thoracic aorta (f) and quantitation of the positive staining area (g) are shown. The black
 1252 scale bar is 200 μ m. (h) Calcium content of the thoracic aorta. (i) Schematic flow
 1253 diagram represented the *in vivo* treatment of CT with or without GW4869 in the VD-
 1254 induced mice model (n = 6 per group). Evaluation of the effect of pre-treatment of the
 1255 exosome blocker GW4869 on arterial calcification induced by VD calcified mice in CT
 1256 treatment. ARS staining (j, l) and RUNX2 expression (k, n) analysis of paraffin-
 1257 embedded vascular tissue from mice. (m) Vascular calcium content measurement. The

1259 black scale bar is 200 μm and the blue scale bar is 50 μm . The data are presented as the
 1260 mean \pm standard deviation with three replicates for each group. The data were analysed
 1261 with Student's t-test or one-way ANOVA with the Bonferroni *post hoc* test. * $p < 0.05$;
 1262 ** $p < 0.01$; *** $p < 0.001$; **** $p < 0.0001$.



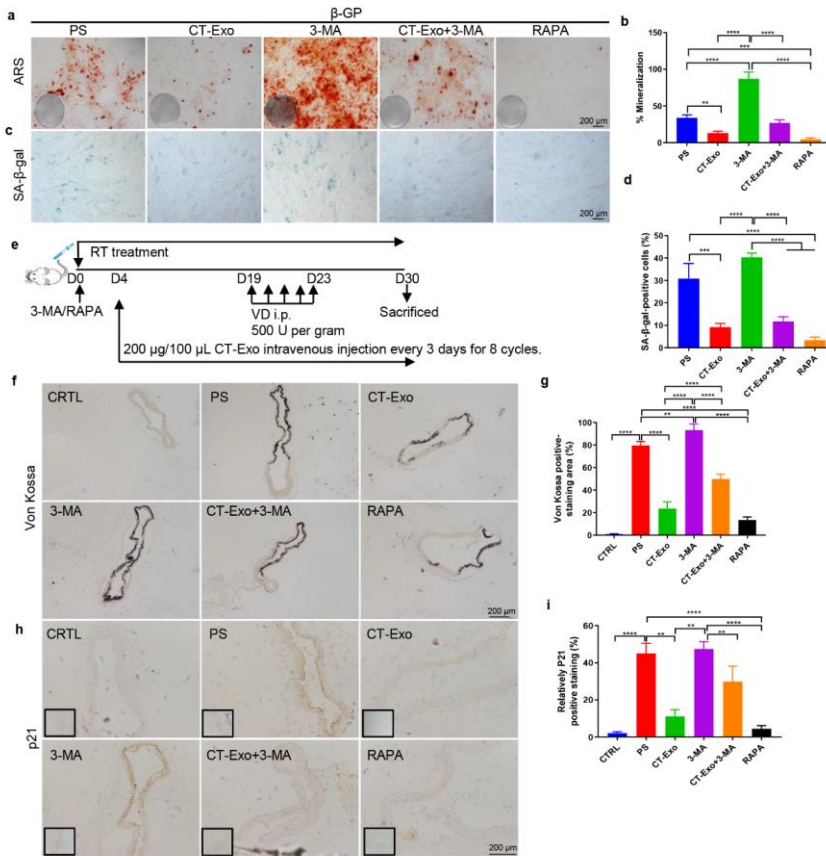
1263
 1264 **Fig. 2 CT-Exo protected against alleviated vascular calcification in the VD-induced**
 1265 **mouse model.** (a) Uptake of DiR-labelled CT-Exo in aortic VSMCs of mice. The mice
 1266 were subjected to the intravenous administration of PBS, DiR or DiR-labelled CT-Exo
 1267 treatments (100 $\mu\text{g}/\text{mice}$, $n = 3$ per group). Representative *in vivo* fluorescence image
 1268 of CT-Exo distribution in mice 24 h after CT-Exo injection. (b) Experimental design of
 1269 the VD-induced vascular calcification mouse model treated with PBS, CT-Exo or RT-
 1270 Exo by intravenous injection ($n = 6$ per group). ARS (c) and Von Kossa staining (d) and
 1271 quantification of the percentages of ARS+ (f) and Von Kossa+ (h) areas. (g) Vascular
 1272 calcium content measurement. RUNX2 expression in thoracic aorta (e) and quantitation
 1273 of positive staining area (i) are shown. The black scale bar is 200 μm and the blue scale

1274 bar is 50 μm . The CTRL group represents the negative control group with only PBS
 1275 treatment. The PS group represents the positive control group with only $\beta\text{-GP}$ treatment.
 1276 The data are presented as the mean \pm standard deviation with three replicates for each
 1277 group. The data were analysed with one-way ANOVA with the Bonferroni *post hoc* test
 1278 or the unpaired, two-tailed Student's t-test. * $p < 0.05$; ** $p < 0.01$; *** $p < 0.001$; **** p
 1279 < 0.0001 .



1280
 1281
 1282 **Fig. 3 CT-Exo protected VSMCs against inhibited the calcification of VSMCs by**
 1283 **promoting autophagy.** (a) Representative fluorescence micrograph of PKH26-labelled
 1284 CT-Exo (red) internalised by VSMCs; nuclei are shown in blue. The white scale bar is
 1285 50 μm . ARS (b) and SA- β -gal (d) staining was evaluated in VSMCs incubated with β -
 1286 GP and CT-Exo for 28 and 10 days, respectively. ~~The n = 5, the~~ black scale bar is 200
 1287 μm . (c, e) The data are presented as ratio of positive staining area. (f) ALP staining was
 1288 measured in VSMCs incubated with β -GP and CT-Exo for 14 days. The black scale bar

1289 is 200 μm . (g) ALP activity. (h) RUNX2 and p53 protein expression was determined by
 1290 western blotting after $\beta\text{-GP}$ and CT-Exo treatment for 3 days. The data are presented as
 1291 densitometric ratios normalised to $\beta\text{-actin}$ (i), $n = 4$. (j, k) Western blots (j) and
 1292 quantification (k) of p62 and LC3B in the PBS, PS and CT-Exo VSMCs, $n = 4$. (l)
 1293 VSMCs were incubated with $\beta\text{-GP}$ and CT-Exo for 72 h and then analysed by electron
 1294 microscopy; a representative image is shown. Autophagosomes containing organelle
 1295 remnants are highlighted by red arrows ($n = 4$ per group). The PS group represents the
 1296 control group with only $\beta\text{-GP}$ treatment. Each experiment was repeated three times. The
 1297 data are presented as the mean \pm standard deviation with three replicates. The data were
 1298 analysed with one-way ANOVA with the Bonferroni *post hoc* test. $*p < 0.05$; $**p <$
 1299 0.01 ; $***p < 0.001$; $****p < 0.0001$.

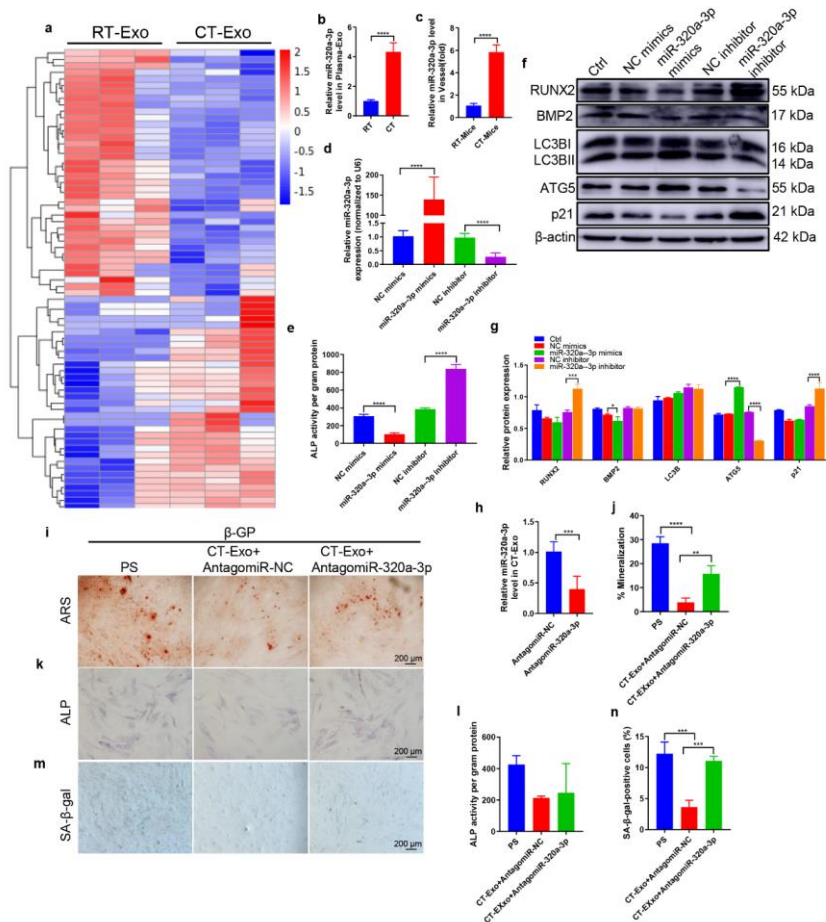


设置了格式: 英语(美国)

1300
 1301 **Fig. 4 3-MA attenuated the pro-aging/pro-calcification preventive effect of CT-Exo**
 1302 **in vitro and in vivo.** Representative images of ARS (a) and SA- β -gal (c) staining of
 1303 VSMCs that had been pre-treated with the indicated concentrations of 3-MA or RAPA

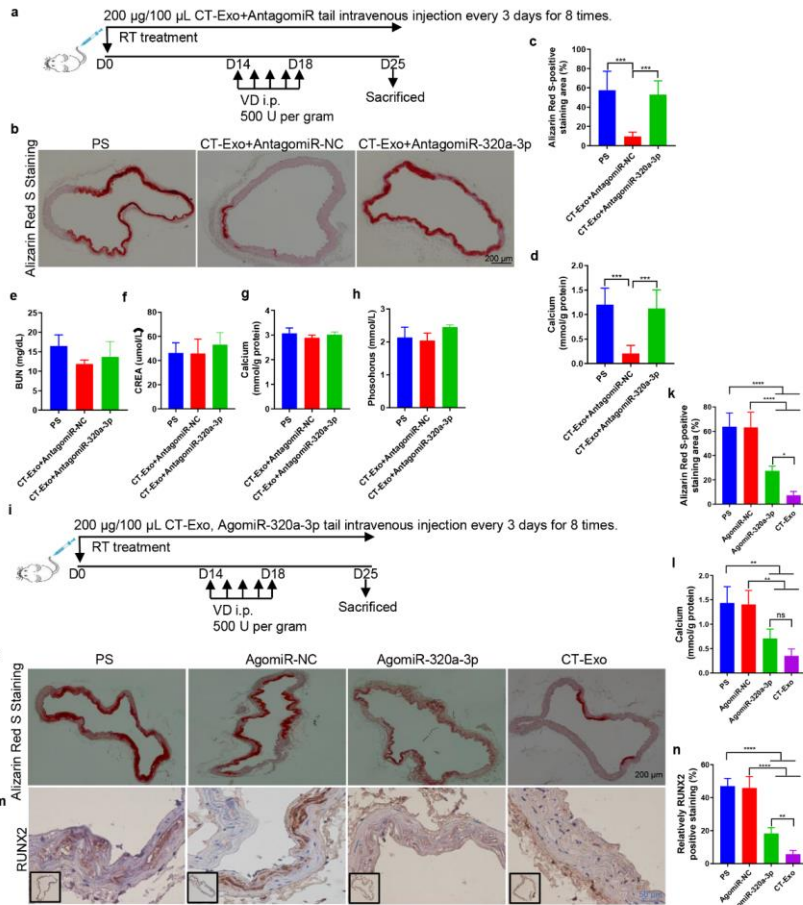
1304 for 30 min and then incubated with β -GP for 28 and 10 days, respectively. ~~The~~ n = 5.
 1305 the scale bar is 200 μ m. Quantitative analysis of the percentages of ARS+ (b, in red)
 1306 and SA- β -gal+ (d, in green) areas. (e) Schematic illustration of the experimental design
 1307 used to assess the effects of CT-Exo and 3-MA on the vascular phenotype in VD-
 1308 induced mice (n = 6 per group). (f, g) Von Kossa staining showed calcified aorta from
 1309 CTRL, PS, CT-Exo, 3-MA, CT-Exo+3-MA and RAPA mice (n = 6 per group). The
 1310 black scale bar is 200 μ m. (h, i) p21 expression in aorta from the six groups of mice
 1311 were examined by immunohistochemistry. The black scale bar is 200 μ m (n = 6 per
 1312 group). The CTRL group represents the negative control group with only PBS treatment.
 1313 The PS group represents the positive control group with only β -GP treatment. The data
 1314 are presented as the mean \pm standard deviation. The data were analysed with one-way
 1315 ANOVA with the Bonferroni *post hoc* test. * $p < 0.05$; ** $p < 0.01$; *** $p < 0.001$; **** p
 1316 < 0.0001 .

1317



1318

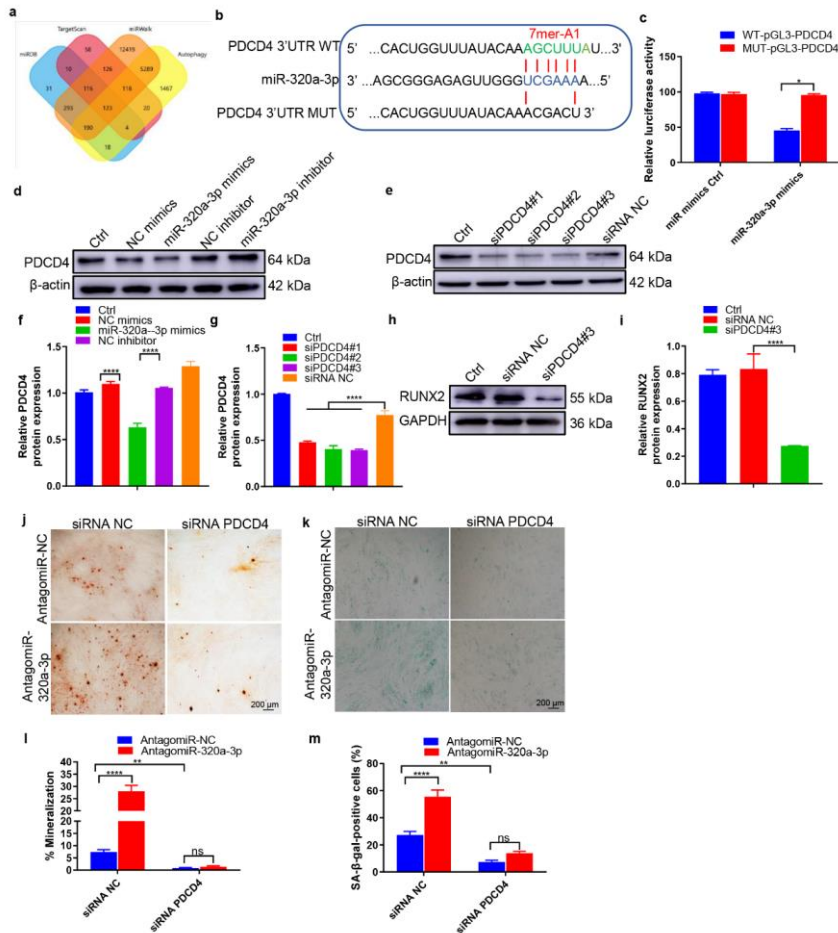
1319 **Fig. 5 miR-320a-3p antagonised osteogenic differentiation of VSMCs.** (a) The
1320 heatmap shows the differentially expressed miRNAs (absolute fold change ≥ 1.5 , $p <$
1321 0.05) between CT-Exo and RT-Exo ($n = 3$ per group). (b) qRT-PCR analysis of miR-
1322 320a-3p expression in exosomes from the plasma of the RT or CT mice ($n = 6$). (c) ~~qRT-~~
1323 ~~PCR analysis of miR-320a-3p expression in vessel s from RT or CT mice ($n = 6$).~~ (d)
1324 qRT-PCR was performed to evaluate the expression of miR-320a-3p in VSMCs
1325 transfected with specific miR-320a-3p mimics or inhibitor ($n = 4$). ~~(d) qRT-PCR~~
1326 ~~analysis of miR-320a-3p expression in vessel s from RT or CT mice.~~ (e) The ALP
1327 activity was evaluated by using specific kits in VSMCs transfected with specific miR-
1328 320a-3p mimics or inhibitors ($n = 4$). (f) Western blotting was performed to determine
1329 the protein expression of RUNX2, BMP2, LC3B, ATG5 and p21 in VSMCs transfected
1330 with specific miR-320a-3p mimics or inhibitors ($n = 4$). (g) The data are presented as
1331 densitometric ratios normalised to β -actin. (h) qRT-PCR analysis of miR-320a-3p
1332 expression in CT-Exo+AntagomiR-320a-3p ($n = 6$). ARS staining (i, j), ALP staining
1333 (k) and ALP activity (l) quantification of SA- β -gal-stained positive cells was shown (m,
1334 n). The black scale bar represents $200 \mu\text{m}$ ($n = 5$ per group). The PS group represents
1335 the positive control group with only β -GP treatment. The data are presented as the mean
1336 \pm standard deviation. The data were analysed with one-way ANOVA with the
1337 Bonferroni *post hoc* test or the unpaired, two-tailed Student's t-test. $*p < 0.05$; $**p <$
1338 0.01 ; $***p < 0.001$; $****p < 0.0001$.



设置了格式: 字体: 倾斜

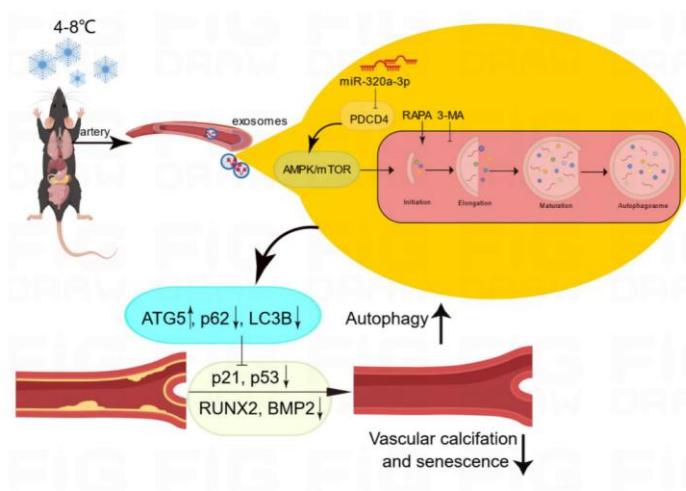
1339
 1340 **Fig. 6 miR-320a-3p effectively protected against inhibited MAC *in vivo* and its**
 1341 **related biochemical indicators.** (a) Experimental design of the VD-induced vascular
 1342 calcification mouse model treated with PBS, CT-Exo+AntagomiR-NC or CT-
 1343 Exo+AntagomiR-320a-3p by intravenous injection (n = 6 per group). ARS staining and
 1344 quantitation (b, c) and vascular calcium content measurement (d). The black scale bar
 1345 is 200 μ m. Serum BUN (e), CREA (f), calcium (g) and phosphate (h) levels in mice
 1346 with VD-induced vascular calcification- (n = 6). (i) Experimental design of the VD-
 1347 induced vascular calcification mouse model treated with PBS, AgomiR-NC or
 1348 AgomiR-320a-3p by intravenous injection (n = 6). ARS staining and quantitation (j, k)
 1349 and vascular calcium content measurement (l). RUNX2 expression in the thoracic aorta
 1350 (m) and quantitation of positive staining area (n) are shown. The black scale bar is 200
 1351 μ m and the blue scale bar is 50 μ m. –The PS group represents the control group with
 1352 only β -GP treatment. The data are presented as the mean \pm standard deviation. The data
 1353 were analysed with one-way ANOVA with the Bonferroni *post hoc* test. ns > 0.05; **p*

1354 < 0.05; ** $p < 0.01$; *** $p < 0.001$ and **** $p < 0.0001$.



1355
 1356 **Fig. 7 PDCD4 is a direct target gene of miR-320a-3p and regulates VSMC calcification.** (a) A Venn diagram showing bioinformatics analysis of miR-
 1357 320a-3p target genes. (b) Schematic representation of miR-320a-3p putative target sites
 1358 in the PDCD4 3'-UTR and the alignment of miR-320a-3p with wild type and mutant
 1359 PDCD4 3'-UTR showing pairing. (c) Luciferase reporter assays were performed using
 1360 luciferase constructs carrying a wild type or mutant PDCD4 3'-UTR co-transfected into
 1361 VSMCs with miR-320a-3p mimics compared with empty vector control. Firefly
 1362 luciferase activity was normalized to Renilla luciferase activity. (d, f)
 1363 PDCD4 protein expression in VSMCs transfected with miR-320a-3p mimics or miR-
 1364 320a-3p inhibitor was determined by western blot (n = 4). (e and g) The efficiency of
 1365 PDCD4 knockdown in VSMCs by siRNA was measured by western blotting (n = 4).
 1366 (h-i) RUNX2 expression was measured in the VSMCs treated with siPDCD4#3 or
 1367 siRNA control (n = 4). (j) ARS staining in β-GP-treated VSMCs transfected with

1369 inhibitors of miR-320a-3p in the presence or absence of PDCD4 siRNA for 28 days;
 1370 representative micrographs are shown. (K) SA- β -gal staining was measured in VSMCs
 1371 incubated with β -GP for 10 days. n = 4. The the data are presented as the ratio of positive
 1372 ARS (j) and SA- β -gal (m) staining area. The scale bar is 200 μ m. The data are presented
 1373 as the mean \pm standard deviation. The data were analysed with one or two-way ANOVA
 1374 with the Bonferroni *post hoc* test. ns > 0.05; **p* < 0.05; ***p* < 0.01; ****p* < 0.001 and
 1375 *****p* < 0.0001.



1376
 1377 **Fig. 8 CT-Exo enrichment of miR-320a-3p under CT exposure can protect against**
 1378 **vascular calcification and senescence by activating autophagy through the**
 1379 **AMPK/mTOR pathway. CT-Exo with the high expression of miR-320a-3p can be**
 1380 **secreted from mice plasma exposed to a cold environment. PDCD4 was found to be a**
 1381 **potential target of miR-320a-3p and to increase osteogenic differentiation and**
 1382 **senescence of VSMCs. CT-Exo can activate AMPK/mTOR, a classical autophagy**
 1383 **pathway and then activate the expression of autophagy proteins (LC3B and ATG5) and**

设置了格式: 字体: 非加粗
 设置了格式: 字体: 非加粗
 设置了格式: 字体: 非加粗
 设置了格式: 字体: 非加粗
 设置了格式: 字体: 非加粗
 设置了格式: 字体: 非加粗

1384 reduce the degradation of autophagy specific substrates (p62). Ultimately, this slow
1385 down the level of senescence (p21 and p53) and decrease the level of calcification
1386 (RUNX2 and BMP2) of VSMCs.

1387

设置了格式: 字体: 非加粗

设置了格式: 字体: 非加粗

设置了格式: 字体: 非加粗

设置了格式: 字体: 非加粗